

Evolutionary SED diagnostics of starburst galaxies: signature of bimodality

T. Takagi^{1,2,3*}, N. Arimoto^{4,5} and H. Hanami⁶

¹ *Blackett Laboratory, Imperial College, Prince Consort Road, London SW7 2BZ, UK*

² *The Institute of Space and Astronautical Science, 3-1-1 Yoshinodai, Sagami-hara, Kanagawa 229-8510, Japan*

³ *Department of Physics, Rikkyo University, 3-34-1 Nishi-Ikebukuro, Toshima-ku, Tokyo 171-8501, Japan*

⁴ *Institute of Astronomy, School of Science, University of Tokyo, 2-21-1 Osawa, Mitaka, Tokyo 181-0015, Japan*

⁵ *National Astronomical Observatory, 2-21-1 Osawa, Mitaka, Tokyo 181-8588, Japan*

⁶ *Physics Section, Faculty of Humanities and Social Sciences, Iwate University, Morioka, 020-8550, Japan*

ABSTRACT

We construct an evolutionary spectral energy distribution (SED) model of a starburst region, from the ultraviolet to submillimetre wavelengths. This model allows us to derive the star formation rate, optical depth by dust and apparent effective radius of starburst regions at various wavelengths; as a result, the intrinsic surface brightness of starburst regions can be derived. Using this SED model, we analyse 16 UV-selected starburst galaxies and 10 ultraluminous infrared galaxies. The derived star formation rates and optical depths are compared with emission line measurements and found to be consistent. The derived apparent effective radii are also consistent with observations. From the SED analysis, we find a bimodal property of the star formation rate with the optical depth and the compactness of stellar distributions. While mild starbursts have a limiting intrinsic surface brightness $L_{bol}r_e^{-2} \simeq 10^{12} L_{\odot}\text{kpc}^{-2}$, intense starbursts tend to be more heavily obscured and concentrated within a characteristic scale of $r_e \simeq 0.3$ kpc. We suggest that the mild starbursts can be triggered by a self-gravitating disc instability in which feedback is effective in the shallow gravitational potential. On the other hand, the intense starbursts can be induced via an external dynamical perturbation like galaxy merging, in which feedback is less effective due to the deep gravitational potential attained by the large gas concentration within the central starburst region.

Key words: galaxies: starburst – dust, extinction – infrared: galaxies – ultraviolet: galaxies – submillimetre.

1 INTRODUCTION

Starbursts are an intensive mode of star formation in galaxies (Storchi-Bergmann, Calzetti & Kinney 1994; Kennicutt 1998). Ultraluminous infrared galaxies (ULIRGs) with $L_{IR} \geq 10^{12} L_{\odot}$ are probably the most active and luminous starburst galaxies. Indeed recent ISO observations suggest that many ULIRGs are powered by starbursts with little contribution from AGN (Genzel et al. 1998; Lutz et al. 1998). On the other hand, starburst galaxies of lower activity are HII galaxies and blue compact dwarf galaxies, known as UV-selected starburst galaxies (UVSBGs; Kinney et al. 1993; Storch-Bergmann et al. 1994; Calzetti, Kinney & Storchi-Bergmann 1994; McQuade, Calzetti & Kinney 1995; Gordon, Calzetti & Witt 1997; Takagi, Arimoto & Vansevičius 1999).

Recently, an upper limit of ‘bolometric surface brightness’ was given by Meurer et al. (1997) for a sample of starburst galaxies observed in the rest frame 1) UV, 2) far infrared (FIR) and $H\alpha$, and 3) 21 cm radio continuum emission. This limit seems to be physically associated with an instability in gaseous discs (e.g. Toomre 1964; Quirk 1972) as Kennicutt (1989) had already suggested for the star formation in normal disc galaxies. In their study, the effective radii are determined from observations at the different wavelengths for each galaxy. However, if a galaxy is optically thick the observed effective radius strongly depends on the degree of extinction, since the observed light comes out solely from the region in which the optical depth is less than unity. Moreover, many ULIRGs have multiple starburst regions (e.g. Scoville et al. 2000; Surace & Sanders 2000), while most of UVSBGs show only one major central starburst region. These effects suggest that the panchromatic intensity

* E-mail: t.takagi@ic.ac.uk

limit on starbursts proposed by Meurer et al. (1997) may not be appropriate for ULIRGs.

To determine the intensity limit of starbursts with various levels of activity ranging from UVSBGs to ULIRGs, it is necessary to estimate both star formation rates (SFRs) and effective radii in a unified manner, whatever the degree of extinction. While typical V -band optical depths in UVSBGs are $\tau_V \sim 0.3 - 2$ (Takagi, Arimoto, & Vansevicius 1999; Storch-Bergmann et al. 1994), those in ULIRGs reach $\tau_V \sim 5 - 50$ (Genzel et al. 1998). Such a wide variation in τ_V causes a serious problem in deriving SFRs, since none of the currently used SFR indicators, such as $H\alpha$ (or other Balmer lines), UV continuum, or FIR luminosities, are commonly applicable for starbursts ranging from UVSBGs to ULIRGs. The FIR luminosity is not a good measure of bolometric luminosity when starburst regions are optically thin, while $H\alpha$ luminosity is difficult to use if the mean surface gas density becomes larger than $50 M_\odot \text{pc}^{-2}$, corresponding to $\tau_V \sim 2$, causing a significant extinction at $H\alpha$ (Kennicutt 1998). What is worse, by using $\text{Br}\gamma$ and FIR luminosities, Kennicutt (1998) has shown that the FIR luminosities give systematically higher SFRs (by a factor of ~ 2) than the $\text{Br}\gamma$ s. Sullivan et al. (2000) compared the $H\alpha$ - and UV-derived SFRs of nearby starbursts to find that starburst galaxies are typically over-luminous in the UV for a given $H\alpha$ luminosity. The effect is strongest in the less luminous galaxies.

When comparing ULIRGs and UVSBGs, the bolometric surface brightness should be derived for each individual starburst region in ULIRGs. The wealth of ground-based low-resolution imaging surveys have provided little information on the stars in the starburst region near the confusion limit $< 1''$. Even the *Hubble Space Telescope (HST)* with its higher resolution $< 0.1''$ fails to go deep enough into the starburst regions, which are obscured by dust at optical wavelengths. The Near-Infrared Camera and Multi-Object Spectrometer (NICMOS) on *HST* can observe the obscured starburst regions more directly at near infrared (NIR) wavelengths where the effects of dust extinction are reduced significantly compared to visual wavelengths. Scoville et al. (2000) studied the morphologies of 24 ULIRGs with NICMOS and found that light profiles of nine of them were well fit by an $r^{1/4}$ law, rather than an exponential profile. The apparent effective radii of ULIRGs tend to be more compact than the extent of gas observed with high-resolution imaging of the CO emission (Bryant & Scoville 1999). This suggests that the distribution of stars is more concentrated than that of dust and gas in the starburst regions. Thus, the dimming of light due to the surrounding dust can be so large that the real distribution of stars deviates from the apparent distribution of the light even the longest observable wavelength with NICMOS of $2.2 \mu\text{m}$.

It is thus crucial to establish a measure of both SFRs and the spatial distribution of stars which can be applied to starbursts of any optical depth. Clearly, a new recipe to derive both SFRs and the stellar distributions is required to investigate the physical properties of starbursts comprehensively.

In this paper, we will use spectral energy distributions (SEDs) from the far ultraviolet (FUV) to submillimetre (submm) to derive SFRs of starburst regions. The SED from the UV to submm can represent the bolometric luminosity,

irrespective of the dust extinction. We construct an ‘evolutionary’ SED model for starburst regions from a simple but realistic point of view. We show that our SED model can explain a wide variety of SEDs from optically thin starbursts (UVSBGs) to optically thick ones (ULIRGs). It is important to note that our SED model can derive not only the SFR, but also the other starburst properties like the optical depth. Moreover, we can derive the apparent effective radius of starbursts at various wavelengths for a given geometry, since we properly take into account the radiative transfer in a dusty medium. Therefore, the evolutionary stages of starburst galaxies can be investigated in a unified manner for a whole range of activity, which can then be compared with the observations of the SED and the effective radius, directly. The systematic estimation of the SFRs and the effective radius can give an answer to the question: is the panchromatic limit of starburst intensity reported by Meurer et al. (1997) also valid for ULIRGs?

This paper is organized as follows. In Section 2, we describe our evolutionary SED model for starburst galaxies. In Section 3, we summarize the model properties. In Section 4, we apply our model to a sample of UVSBGs and ULIRGs in the local Universe and describe the resulting properties of nearby starburst galaxies derived from our SED model fitting. Sections 5 and 6 give discussions and conclusions, respectively.

2 EVOLUTIONARY SED MODEL FOR STARBURST REGIONS

2.1 Star formation and chemical evolution

We consider a model for the chemical enrichment of a starburst region into which gas is supplied continuously. When a large amount of gas is supplied into the central region of a galaxy, a starburst is triggered. Since the details of the gas supplying mechanism are yet to be investigated, it would not be outrageous to suppose that star formation and chemical evolution in the starburst regions are approximately described by an infall model of chemical evolution (Arimoto, et al. 1992). Ubiquitous galactic outflows from the starbursts have been observed with the X-ray emission from the hot gas driving the flow, optical line emission produced by the warm gas, and the interstellar absorption lines (e.g. Heckman et al. 2000; Lehnert & Heckman 1996). Heckman et al. (2000) suggested that most of the outflow gas consists of ambient material which has been ‘mass-loaded’ into the hot gas. Therefore, we assume that the amount of gas in the outflow from a starburst region has negligible impact on the chemical evolution as a whole. This is true if the mass loss rate from a starburst region is less than 10% of the SFR. Under this simple evolutionary picture, a starburst is characterized by the rates of gas infall and star formation.

The time variation of gas mass $M_g(t)$, total stellar mass $M_*(t)$, and gas metallicity $Z_g(t)$ are given by the equations:

$$\frac{dM_g(t)}{dt} = -\psi(t) + E(t) + \xi_i(t), \quad (1)$$

$$\frac{dM_*(t)}{dt} = \psi(t) - E(t), \quad (2)$$

$$\frac{d(Z_g M_g)}{dt} = -\psi(t)Z_g(t) + E_Z(t) + \xi_i(t)Z_i, \quad (3)$$

where $E(t)$, $E_Z(t)$, and Z_i are the ejection rates of the gas and the metals from dying stars, and the metallicity of the supplied gas, respectively. We set the initial condition as $M_g(0) = M_*(0) = 0$ for all the calculations in this paper. Although some amount of gas and stars unrelated to the starbursts are initially expected in the starburst region, we assume that the amount of initial gas and stars are negligible in both the chemical and photometric evolution of starburst region. For Z_i , the star formation history before the starburst event is important. We will explicitly note the adopted values of Z_i later. We assume Z_i is constant during the starburst event.

The SFR $\psi(t)$ is given by

$$\psi(t) = \frac{1}{t_*} M_g(t), \quad (4)$$

where t_* and $M_g(t)$ are the star formation time-scale and the gas mass in the starburst region, respectively. The gas supply rate is given by:

$$\xi_i(t) = \frac{M_T}{t_i} \exp\left(-\frac{t}{t_i}\right), \quad (5)$$

where M_T and t_i are the initial gas mass in the reservoir surrounding the starburst region and the time-scale of gas supply, respectively (Arimoto et al. 1992). Physically, the time-scales t_i and t_* can be expressed in terms of the dynamical time, sound-crossing time, and cooling time, depending on what triggers the starburst. It is however difficult to ascertain the characteristic time-scale of each starburst from observations. Thus, we hereafter analyse the simplest case, in which a starburst is characterized by only one evolutionary time-scale t_0 , i.e., we adopt $t_0 \equiv t_i = t_*$.

For all cases in this paper, we adopt the Salpeter initial mass function (IMF) with the lower and upper mass limit of $0.1 M_\odot$ and $60 M_\odot$, respectively. Equations (1)-(3) are numerically solved by using an evolutionary population synthesis code of Kodama & Arimoto (1997). The adopted stellar libraries and evolutionary tracks are the same as those in the original code. Details of nucleosynthesis prescription is given there.

The effect of dust on the SEDs is significant and predominant in starburst regions. In this paper, we adopt a simple model in which the dust-to-metal ratio δ_0 is constant; i.e., $M_D(t) = \delta_0 Z_g(t) M_g(t)$. As described below (Section 2.3), we use three types of dust model for the Milky Way (MW), Large and Small Magellanic Clouds (LMC; SMC). The adopted values of δ_0 for MW, LMC and SMC are 0.40, 0.55, 0.75, respectively (Takagi 2001). Starbursts could be the most ideal case for constant $\delta(t)$, since 1) only type II supernovae contribute to the supernova rate and 2) the gas fraction in molecular clouds is large (see Dwek 1998).

2.2 Model geometry of starburst region

We consider a starburst region in which stars and dust are distributed within a radius r_t . We introduce a mass-radius relation for the starburst region;

$$\frac{r_t}{1\text{kpc}} = \Theta \left(\frac{M_*}{10^9 M_\odot} \right)^\gamma, \quad (6)$$

where Θ is a compactness factor which expresses the matter concentration; the mean density becomes higher for smaller

Θ . Starburst galaxies are characterized by a large surface brightness, which are roughly constant (Armus, Heckman & Miley 1990; Meurer et al. 1995, 1997). In the adopted mass-radius relation, $\gamma = 1/2$ gives the constant surface brightness for constant Θ . Therefore, we adopt $\gamma = 1/2$ throughout this paper. A variation in the surface brightness can be expressed by the different values of Θ in our model. Note that not only the surface brightness but also the SED feature is preserved for different values of M_* if $\gamma = 1/2$, since the source function within the starburst is conserved. Therefore, multiple systems with the total stellar mass of M_* , in which each component has the same surface brightness, have the same SED as that of a unit system with a stellar mass of M_* .

We assume that the stellar density distribution $\rho(r)$ is given by a generalized King profile;

$$\rho(r) = \rho_0 \left[1 + \left(\frac{r}{r_c} \right)^2 \right]^{-\beta}, \quad (7)$$

where ρ_0 is the stellar density at the centre of starburst region and r_c is a core radius of stars. We adopt the stellar density distribution of typical elliptical galaxies; i.e., the concentration parameter $c \equiv \log(r_t/r_c) = 2.2$, and $\beta = \frac{3}{2}$ (Combes et al. 1995). Recently, Scoville et al. (2000) and James et al. (1999) presented K -band images of starburst galaxies, and demonstrated that luminosity profiles of starbursts are well represented by the $r^{1/4}$ profile which is quite similar to those of elliptical galaxies. However, in order to derive the stellar density distribution in starbursts, it is important to eliminate the effects of dust extinction, since the effect of radiative transfer can easily alter the luminosity profile from the original one. As we will show later, this effect is not negligible even in the K -band in ULIRGs (see Section 3.3). Therefore, the true density distribution of stars in starburst galaxies is difficult to determine directly, and we therefore adopt the typical density profile of elliptical galaxies as a first guess. This topic is further discussed in Section 3.3 and 4.4.

Following Takagi et al. (1999), we assume that dust is distributed homogeneously within a radius r_t of the starburst region. It is plausible that the dust distributes more diffusely than the stars, due to feedback from supernovae. When the light from centrally concentrated stars dominates the SED, i.e., optically thin case, this geometry results in a similar SED to the case of shell geometry, which is suggested for UVSBGs by Gordon et al. (1997), Meurer, Heckman & Calzetti (1999), Witt & Gordon (2000). However, in the optically thick case, like ULIRGs, the shell geometry results in the spectral cut-off around NIR (see the results by Rowan-Robinson & Efstathiou 1993), and therefore UV-NIR SED of ULIRGs cannot be reproduced with this geometry without invoking the other components, like underlying stellar populations and/or AGNs. As we show in Section 4.2, our model can essentially reproduce UV-NIR SEDs of ULIRGs only with starburst stellar populations. These SED fitting results are confirmed with emission line measurements and the observed effective radii in Section 4.3 and 4.4, respectively. Therefore, we believe that the adopted geometry is suitable to approximate the real geometry of starburst regions with various optical depths.

2.3 Dust model

The dust model is adopted from Takagi (2001) who successfully reproduced the extinction curves observed in MW, LMC and SMC, as well as the spectrum of Galactic cirrus. The difference among the MW, LMC and SMC extinction curves is attributed to the variation of the ratio of carbonaceous dust (graphite and PAHs) to silicate grains.

The extinction curve is given by the cross-section per hydrogen:

$$\sigma_{0\lambda}^H = \frac{1}{n_H} \sum_k \int \sigma_{\lambda,k}^e(a) \frac{dn_k}{da} da, \quad (8)$$

where n_H is the number density of hydrogen, $\sigma_{\lambda,k}^e(a)$ is the extinction-cross section of dust particle with the dust constituent k and size a . The size distribution of each dust constituent dn_k/da is taken from Takagi (2001). For a constant dust-to-metal ratio, the extinction curve at starburst age t is given by:

$$\sigma_{\lambda}^H(t) = \frac{Z^H(t)}{Z_0^H} \sigma_{0\lambda}^H, \quad (9)$$

where $Z^H(t)$ is the gas metallicity with respect to hydrogen mass (as opposed to the total gas mass) and Z_0^H is the metallicity of the ISM under the same definition. We adopt $Z_0^H = 0.024, 0.011, 0.0034$ for the MW, LMC and SMC extinction curves, respectively (Pagel 1997; Lequeux et al. 1979). The time variation of optical depth $\tau_V(t)$ is given by $n_H(t)\sigma_{\lambda}^H(t)r_t(t)$. Note that $r_t(t)$ is defined by the time dependent total stellar mass $M_*(t)$. According to the adopted mass-radius relation, $\tau_V \propto n_H r_t \propto M_H r_t^{-2} \propto f_H M_T r_t^{-2} \propto f_H M_T (f_{star} M_T)^{-1} \propto f_H f_{star}^{-1}$ where M_H and f_H are the total mass of hydrogen and the mass fraction of hydrogen, respectively; therefore, τ_V does not depend on the value of M_T .

2.4 Intrinsic SED and radiative transfer

We calculate unobscured stellar SEDs by using the population synthesis code of Kodama & Arimoto (1997), in which the effect of stellar metallicity is fully taken into account. We solve the equation of radiative transfer by using a computational code developed by Takagi (2001). Isotropic multiple scattering is assumed and the self-absorption of re-emitted energy from dust is fully taken into account. The temperature fluctuation of very small dust particles is calculated consistently with the radiative transfer.

We assume no gradient of the stellar population along the radius of starburst region. Although gas emission is not considered in our model, a modification of the total SED due to gas emission is not significant unless a starburst is considerably younger than 10 Myr (Leitherer & Heckman 1995; Fioc & Rocca-Volmerange 1997). The contribution from gas emission to the continuum light is especially important in the NIR. As we will show later, no systematic discrepancies in the NIR flux are found between model results and observations. Therefore, we believe that starburst galaxies are old enough to have negligible contribution from gas emission to the continuum.

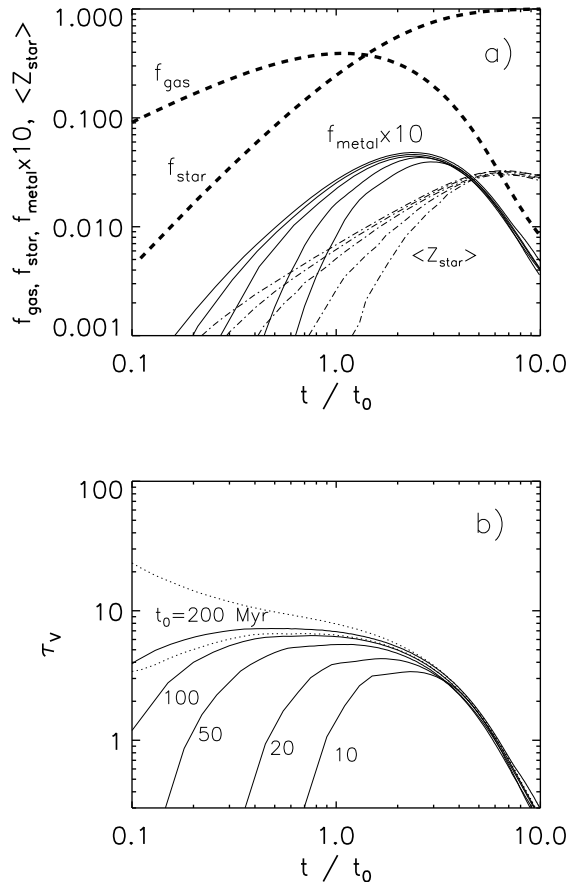


Figure 1. Chemical evolution for $t_0 = 10, 20, 50, 100$ and 200 Myr with $Z_i = 0$. a) Evolution of gas mass fraction f_{gas} , stellar mass fraction f_{star} , and metal mass fraction f_{metal} . Both f_{gas} and f_{star} are almost independent of t_0 so that the variation of both quantities is no more than the thickness of dashed curves. Luminosity-weighted mean stellar metallicities are indicated by dot-dashed lines. b) Evolution of optical depth at V-band. For two dotted lines, the different values of Z_i ($0.01Z_{\odot}$ for lower and $0.1Z_{\odot}$ for upper) are adopted with $t_0 = 100$ Myr.

3 MODEL PROPERTIES

3.1 Evolutionary properties

Fig. 1 shows how chemical properties and τ_V evolve as a function of t/t_0 , for $t_0 = 10, 20, 50, 100$, and 200 Myr. The gas mass fraction f_{gas} , stellar mass fraction f_{star} , and metal mass fraction f_{metal} are defined as M_g/M_T , M_*/M_T , and $Z_g M_g/M_T$, respectively. The luminosity-weighted mean metallicity is expressed as (Arimoto & Yoshii 1987):

$$\langle Z_{\text{star}} \rangle = \frac{\sum Z_{\text{star}} L_{\text{star}}}{\sum L_{\text{star}}}, \quad (10)$$

where Z_{star} and L_{star} are the metallicity and luminosity of each star, respectively. In this section, we simply adopt $Z_i = 0$, unless otherwise explicitly noted.

The variation of f_{gas} and f_{star} as a function of t/t_0 is almost independent of t_0 . After $t/t_0 \approx 2$, the evolution of f_{metal} ($\equiv f_{\text{gas}} Z_g$) and τ_V depend little on t_0 . Dust mass evolves in proportion to f_{metal} , but τ_V evolves somewhat

differently, since r_t increases gradually as stellar mass accumulates. The effect of Z_i on τ_V is negligible for $t/t_0 > 1$.

Fig. 2 shows the evolution of L_{bol} , L_{IR} , $\psi(t)/L_{bol}$, L_{FIR}/L_H , $B-H$, τ_V^{eff} , and T_D^{eff} . τ_V^{eff} is the effective optical depth at V-band defined as $L_V = L_V^0 \exp(-\tau_V^{eff})$, where L_V^0 and L_V are the intrinsic and attenuated luminosity, respectively. T_D^{eff} is the effective dust temperature which gives the same peak wavelength of dust emission as that of a model SED with an emissivity law $\propto \lambda^{-2}$.

We summarize the model properties as follows:

1) The IR luminosity evolution suggests that starburst galaxies should be found mostly in the late phase ($t/t_0 \gtrsim 2$), after the SFR and the dust mass become maximum. The asymptotic relation between SFR $\psi(t)$ and L_{bol} for the late phase $t/t_0 > 2$ is

$$\frac{L_{bol}}{1.7 \times 10^9 L_\odot} = \frac{\psi(t)}{1 \text{M}_\odot \text{yr}^{-1}} \frac{t}{t_0}. \quad (11)$$

We also derive an asymptotic relation for the mass-to-light ratio for the late phase $t/t_0 > 2$;

$$\frac{M_*}{L_{bol}} = 8.05 \times 10^{-3} \left(\frac{t}{t_0}\right)^{1.8} \left(\frac{t_0}{100 \text{Myr}}\right)^{0.8} \frac{M_\odot}{L_\odot}. \quad (12)$$

These ratios will be used in the analysis of starbursts later (Section 5).

2) The variation of L_{FIR}/L_H as a function of t/t_0 is nearly independent of t_0 . L_{FIR}/L_H decreases monotonically with time. Due to this weak dependence of SED quantities on t_0 , it is difficult to determine the absolute starburst age from the SED fitting alone.

3) The dependence of $B-H$ on t_0 is similar to that of τ_V and τ_V^{eff} .

Fig. 3 shows the SED evolution for $t_0 = 100$ Myr, $\Theta = 1$, the MW extinction curve, and $Z_i = 0$. The SEDs are quite similar to each other at $t/t_0 < 2$. At $t/t_0 > 2$, the peak wavelength of dust emission increases and the FIR excess (L_{FIR}/L_H) decreases.

3.2 Dependence on compactness factor

Fig. 4 shows how the characteristic SED quantities depend on the compactness factor Θ . While L_{FIR} is not sensitive to Θ , L_{FIR}/L_H increases significantly for $\Theta < 1$. At a small Θ (i.e., optically thick), the SED at optical wavelengths asymptotically reaches the source function of the stellar light, since the light mainly comes from near the surface for such a highly obscured region. This is the reason why a starburst region becomes bluer for $\Theta \lesssim 0.5$.

There are two possible reasons for large values of τ_V ; 1) starbursts occur in metal rich clouds ($Z_i > 0.1 Z_\odot$) and are still very young ($t/t_0 < 0.3$) as shown in Fig. 1b, and 2) geometry of starbursts is compact ($\Theta < 1$) as shown in Fig. 4d. If the former reason is the case, ULIRGs should be younger than UVSBGs, systematically. However, we find no such systematic difference as we show in Section 4. Instead, SED fitting results in smaller Θ for ULIRGs than those of UVSBGs. Thus, the variation of τ_V in starbursts is mainly caused by the geometrical effect; i.e., Θ . This result is reasonable, since the luminosity evolution suggests that starbursts are less luminous in the early phase of starbursts. In later phases, the high luminosity and large fraction of

life time during this phase as a starburst would increase the chance of the starbursts being observed. The importance of Θ on the variation in starburst SED is illustrated clearly in Fig. 5.

3.3 Effective radius in various wavelengths

Fig. 6 shows the growth curve of the apparent surface brightness at 0.22, 0.7, 1.1, 2.2, and 100 μm for the models of UVSBGs ($t/t_0 = 2.0$, $\Theta = 1.5$ and the MW extinction curve) and ULIRGs ($t/t_0 = 2.0$, $\Theta = 0.4$ and the SMC extinction curve). Here we adopt the typical values of model parameters for each UVSBGs and ULIRGs, which are derived from the SED fitting described in the next section. At most of the observed wavelengths, as seen in Fig. 6, the apparent effective radii are systematically larger than the intrinsic effective radius which corresponds to the case without any extinction. In the FUV to NIR wavelength region in which the dust emission is negligible, the apparent effective radius increases with decreasing wavelength. This is because the contribution from stars in the central region decreases with increasing optical depth toward the shorter wavelength region. Therefore, only the growth curve in 2.2 μm follows that of the input stellar distribution for the case of UVSBGs. Meurer et al. (1995) presented the surface brightnesses of UVSBGs at FUV (0.22 μm) obtained with the *HST*/Faint Object Camera (FOC). These surface brightness is not well represented by the $r^{1/4}$ or exponential profile. This result is consistent with the model for UVSBGs in which the growth curve at 0.22 μm is significantly different from the intrinsic growth curve (dashed line). Note that both the $r^{1/4}$ and exponential profile have been used for normal galaxies in which the effect of dust is not significant, compared to starburst galaxies. On the other hand, in the case of ULIRGs, the apparent effective radius even at 2.2 μm becomes twice the intrinsic effective radius, although the growth curve is somewhat similar to the intrinsic one. In both UVSBGs and ULIRGs, the effect of scattering on the growth curve is negligible. The apparent effective radius at 100 μm is also different from the intrinsic effective radius, since it is determined by the distribution of dust, rather than that of stars.

4 SED FITTING TO UVSBGs AND ULIRGS

We apply our evolutionary SED model to two samples of local starburst galaxies; UVSBGs and ULIRGs. All models are calculated with $t_0 = 100$ Myr, $Z_i = 0.1 Z_\odot$. A definitive value of t_0 is only important for the absolute time scale of starburst events which is not discussed here. The value of Z_i should vary for each starburst galaxy, since Z_i depends on the star formation history in precursors of a starburst galaxy. We expect that the gas fraction in precursors of starbursts should be large, and therefore assume that the level of chemical enrichment in precursors is low and comparable to that in the SMC. Our conclusions are independent of the choice of Z_i .

Fitting parameters are the starburst age t , and the compactness factor Θ . We choose the best-fitting extinction curve from the MW, LMC and SMC type. The SEDs are normalized by the initial mass M_T of a gas reservoir. The best-fitting model for each galaxy is sought by a standard

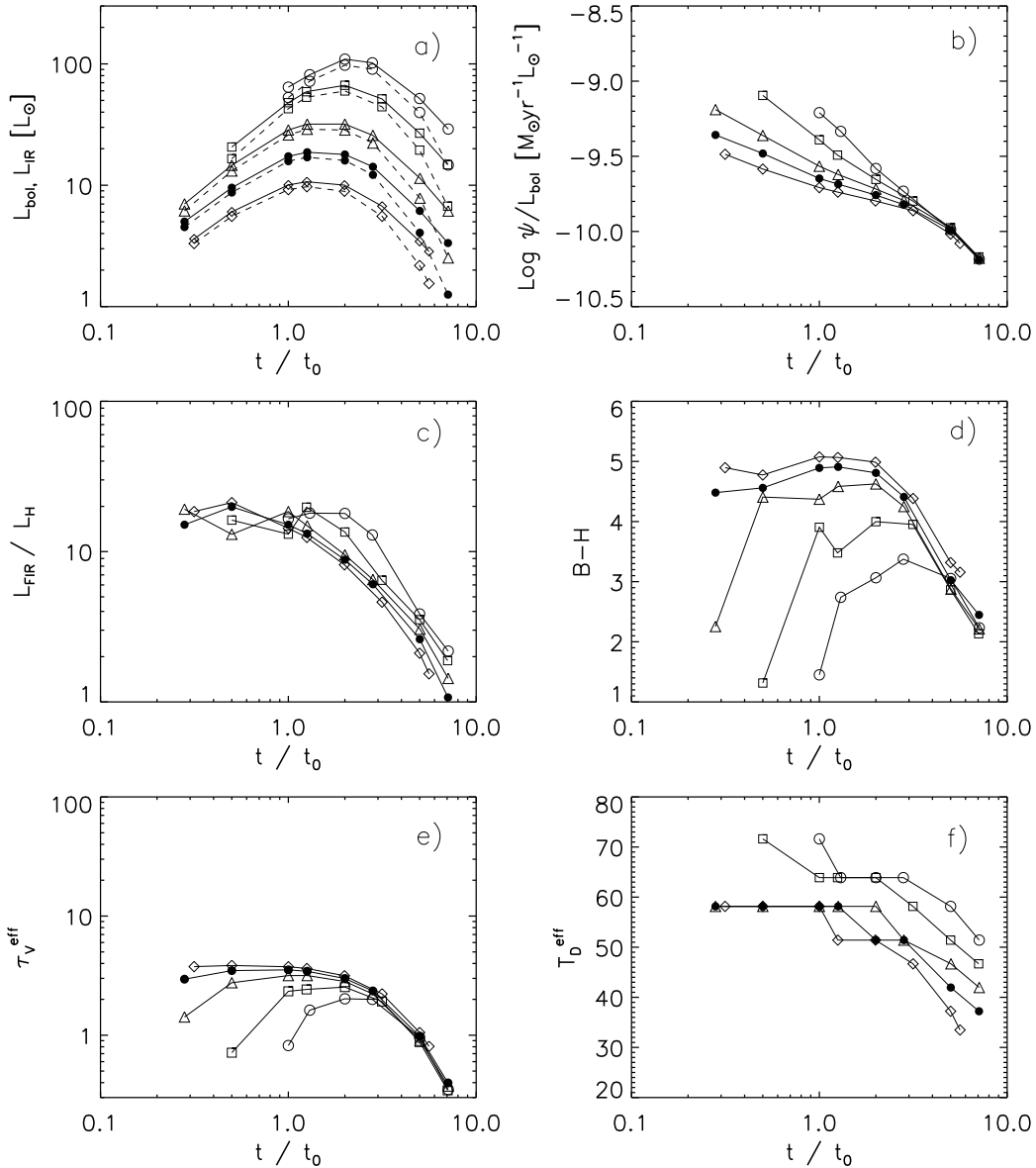


Figure 2. The evolution of characteristic quantities of starburst galaxies, a) L_{bol} (solid line) and L_{IR} (dashed line), b) the ratio of SFR to L_{bol} , c) L_{FIR}/L_H , d) $B-H$, e) τ_V^{eff} , f) effective temperature of dust T_D^{eff} for various t_0 (open circles for $t_0 = 10$ Myr, squares for 20 Myr, triangles for 50 Myr, solid circles for 100 Myr, and diamonds for 200 Myr). L_{IR} and L_{FIR} are the luminosity in the wavelength range of $8 - 1000 \mu\text{m}$ and $42 - 122 \mu\text{m}$, respectively. We adopt the MW extinction curve, $\Theta = 1$, $M_T = 1 M_{\odot}$ and $Z_i = 0.0$.

least square method. We adopt the cosmology of $H_0 = 75 \text{ km sec}^{-1} \text{ Mpc}^{-1}$ and $q_0 = 0.5$ throughout this paper.

4.1 UVSBGs

We analyse the same sample of UVSBGs analysed by Takagi et al. (1999). Photometric data from FUV to NIR are taken from Gordon et al. (1997) who presented a homogeneous sample of aperture-matched SEDs of 30 starburst galaxies. All of the sample was detected by the *IUE* satellite. UV-selected starbursts are relatively bright in the UV and expected to be less attenuated by dust. The aperture size of the FUV-NIR photometry is $10'' \times 20''$, which is equal to $\sim 4.5 \text{ kpc}$ at their median distance of 60 Mpc. The IRAS flux

densities are taken from NED (NASA/IPAC Extragalactic Database). The IRAS fluxes are derived for the total galaxy, while the UV-NIR photometric data are aperture limited in the central region of starburst galaxies on average. Nevertheless, the aperture correction does not change our main conclusions, since the FIR emissions tend to concentrate at galactic centre in the galaxies analysed here (Calzetti et al. 1995). We fit the SEDs of 16 galaxies out of 30, which were detected in all four IRAS bands ($12\mu\text{m}$, $25\mu\text{m}$, $60\mu\text{m}$ and $100\mu\text{m}$).

First, the best-fitting model is determined by the SED fitting from the *U*-band to the FIR, i.e., without FUV data obtained with the *IUE* satellite. The fitting results from the *U*-band to the FIR are shown in Fig. 7 with dashed lines.

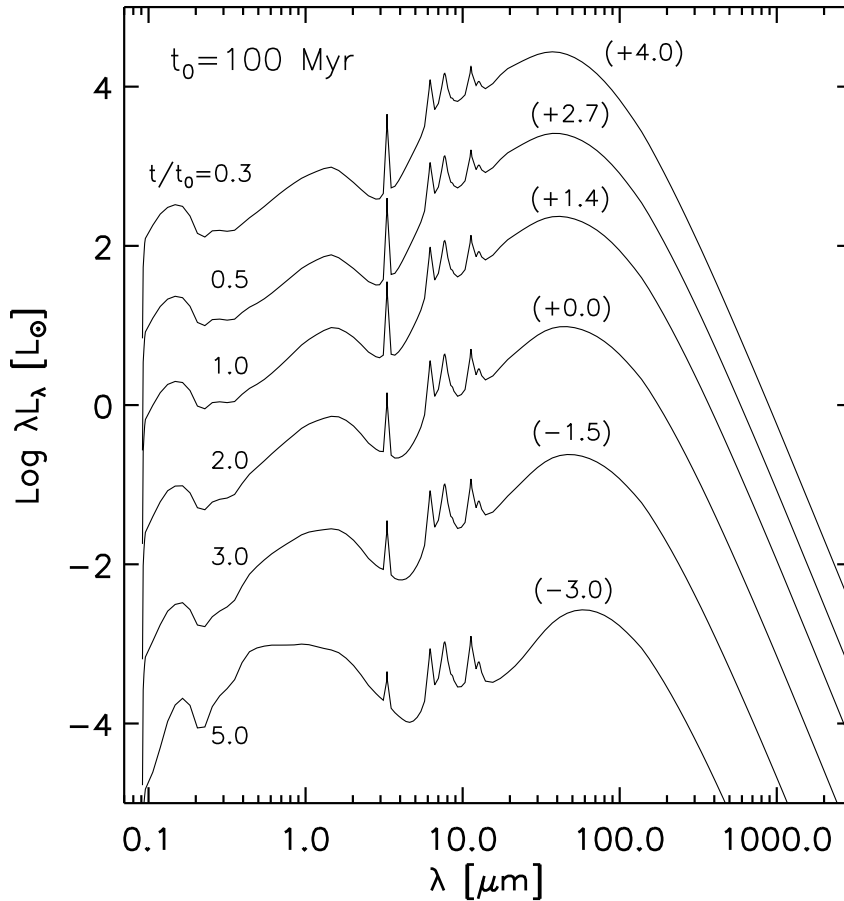


Figure 3. The spectral evolution of a starburst for $\Theta = 1$ with $M_T = 1 M_\odot$, the MW extinction curve and $Z_i = 0$. The evolutionary stage for each line is denoted near the lines. For clarity, the SEDs are shifted vertically with the denoted value in parenthesis at the emission peak.

All the best-fitting models result either in reasonable fits or in underestimates to the FUV data.

This discrepancy in the FUV flux can be reasonably explained by the effect of photon leakage. Although we consider a homogeneous distribution of dust, regions with low gas density are naturally expected in the starbursts, because of a cavity produced by successive supernova explosions, for example. The effect of photon leakage is expected to be more significant in the FUV compared with the longer wavelength region, since the starburst population is intrinsically luminous in the FUV. Therefore, the fitting results are consistent with our proposed picture of the starburst region.

We estimate the effect of photon leakage as follows. Although various levels of extinction for leaking photons are expected, depending on the degree of inhomogeneity in the dust distribution, the contribution of leaking photons from optically thinner regions could be much more significant. Therefore, for simplicity we assume that the extinction of leaking photons is negligible. We define the energy fraction of photons which leak out from the stars directly through the starburst region, f_{leak} , as:

$$F_\lambda^{\text{obs}} = (1 - f_{\text{leak}})F_\lambda(\tau_\lambda) + f_{\text{leak}}F_\lambda(\tau_\lambda = 0), \quad (13)$$

where F_λ^{obs} is the observed flux, and $F_\lambda(\tau_\lambda)$ is the model flux for a given optical depth without considering the photon leakage. By using $F_\lambda(\tau_\lambda)$ and $F_\lambda(\tau_\lambda = 0)$ for each starburst galaxy derived from the U -band to FIR SED (i.e., without FUV data), we determine the most plausible value of f_{leak} by the least square method by using all photometric data including the FUV; i.e., in this fitting process, we use f_{leak} as a free parameter. Also, M_T is re-adjusted to give the least square value for the SED with the leakage correction, which is necessary to derive a more accurate bolometric luminosity, and therefore SFR.

The best-fitting models with the photon leakage are indicated by solid lines in Fig. 7. As a whole, these models show a good agreement with the observed SEDs. For most of the sample galaxies, the SEDs in the FUV can be reproduced with a f_{leak} less than 0.1. Note that the correction of SED due to the photon leakage effects only the FUV. In Table 1, the best-fitting parameters are given together with the resulting L_{bol} , M_* , M_D , SFR and τ_V^{eff} . From the SED fittings with our adopted evolutionary time-scale $t_0 = 100$ Myr, most of the derived starburst ages are within 200–400 Myr. As we already noticed, starbursts are most luminous during the ages of $t/t_0 \simeq 2 - 4$. Therefore, the derived ages

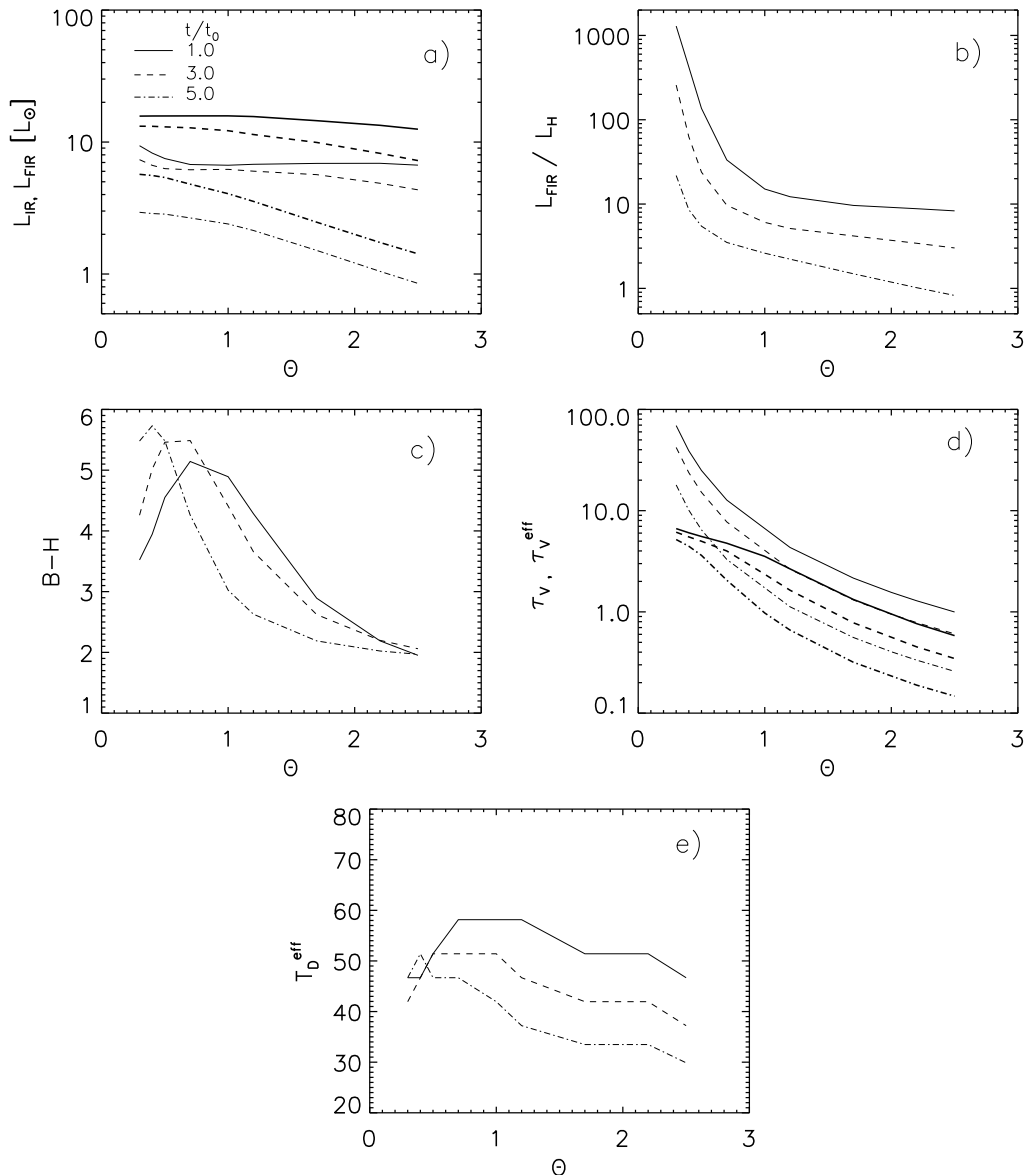


Figure 4. The dependence of a) L_{FIR} (thin lines) and L_{IR} (thick lines), b) L_{FIR}/L_H , c) $B - H$, d) τ_V (thin lines) and τ_V^{eff} (thick lines), e) T_D^{eff} on Θ . The case for $t_0 = 100$ Myr are shown in each panel. Solid, dashed and dot-dashed lines indicate the case of $t/t_0 = 1.0$, 3.0 and 5.0, respectively. We adopt the MW extinction curve, $M_T = 1 M_\odot$, and $Z_i = 0.0$.

with the SED fittings are reasonable for the starbursts. For all the sample but three, we found that the MW extinction curve is most suitable for UVSBGs. Note that the absorption feature at 2175\AA is not used to determine the extinction curve. The MIR colours are important for the resulting extinction curve, since the difference in the relative fraction of dust constituents can effect the MIR SED in which very small graphite grains and PAHs play significant role. The mean value of Θ is 1.6, corresponding to $\tau_V^{\text{eff}} = 1.2$ for $t/t_0 = 2.0$ in the case of the MW extinction curve.

Some galaxies, such as NGC5236, NGC6052 and NGC6217, show a notable excess of $100\ \mu\text{m}$ flux compared to the model SEDs. As we noted, the aperture size adopted for IRAS data is larger than those of the FUV – NIR data. Therefore, it is likely that the FIR emission from cold dust,

heated by the interstellar radiation field generated by the underlying stellar populations, contributes to the $100\ \mu\text{m}$ flux.

For IC214, the model with the photon leakage still underestimates the FUV fluxes. Since this galaxy along with NGC1614 is the faintest in FUV among the UVSBG sample, the signal-to-noise ratio of the *IUE* observation is low (3.2 for 1515\AA ; Kinney et al. 1993). A more sensitive observation would be necessary for a detailed discussion on the origin of this discrepancy.

4.2 ULIRGs

The sample of galaxies with $L_{IR} > 10^{12} L_\odot$, i.e., ULIRGs, analysed here were originally studied by Sanders et al.

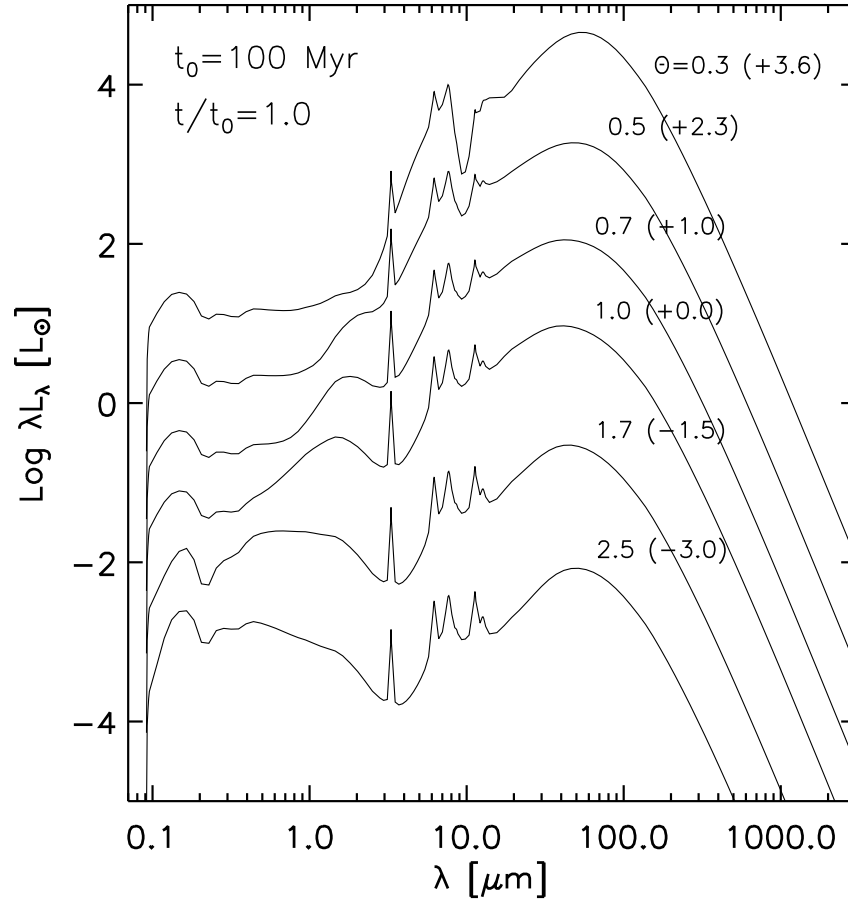


Figure 5. The SEDs of starburst galaxies for various Θ with $M_T=1 M_\odot$. We adopt the MW extinction curve and $Z_i = 0$. For clarity, the SEDs are shifted vertically with the denoted value in parenthesis, following the values of θ .

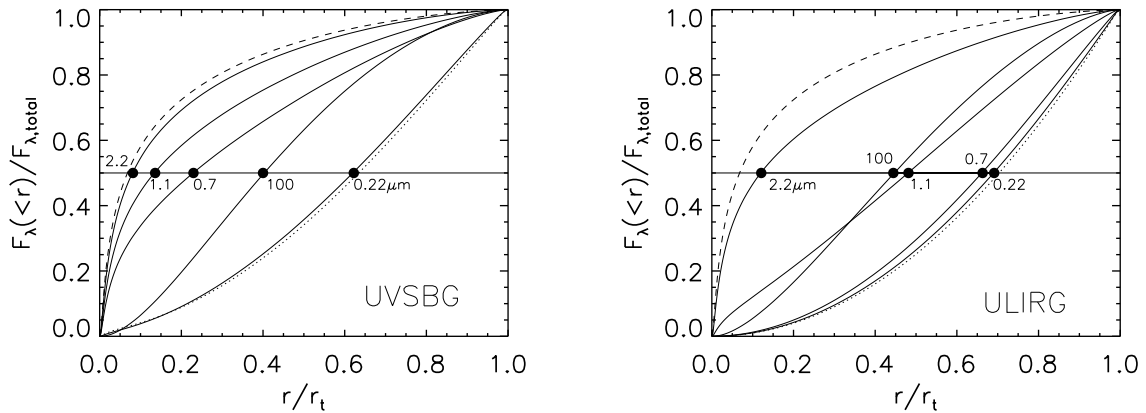


Figure 6. Growth curves of starburst region at various wavelengths. The vertical axis is the fraction of flux emitted within the projected radius r . Dashed line is for the case without dust. Effective radii for each wavelength is indicated by solid circles. Dotted line indicates the growth curve at $0.22 \mu\text{m}$ without a contribution from scattering light. Left panel: the case for UVSBGs ($t/t_0 = 2.0$, $\Theta = 1.5$ and the MW extinction curve), right panel: the case for ULIRGs ($t/t_0 = 2.0$, $\Theta = 0.4$ and the SMC extinction curve).

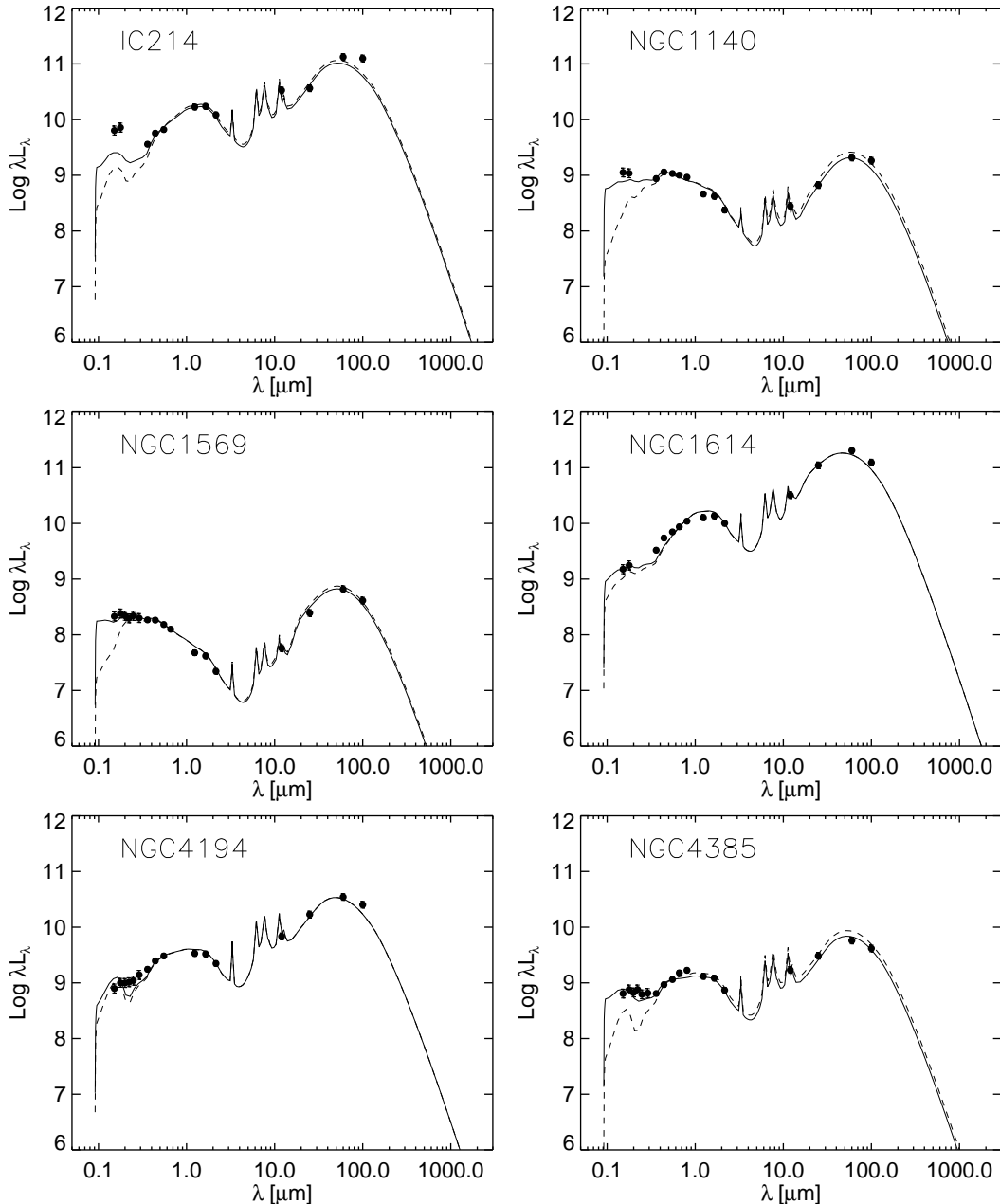


Figure 7. Fitting results for UV-selected starburst galaxies. The dashed lines indicate the fitting results without taking into account the photon leakage. In this case, we fit the model SEDs to observations, except for FUV data. The solid lines are the best-fitting models for observed SEDs including the FUV data, considering the photon leakage. λL_λ is in solar unit.

(1988). Although a starburst is the only energy source in our model, we also apply it to Seyfert galaxies in which the AGN could considerably contribute to the dust heating. According to Veilleux et al. (1999a), IRAS05189, Mrk231 and Mrk273 are Seyfert galaxies, although the line-to-continuum ratio of the $7.7 \mu\text{m}$ emission feature indicates that Mrk273 is a starburst-dominated ULIRG (Rigopoulou et al. 1999).

All photometric data from the B -band to the submm wavelengths are taken from Rigopoulou, Lawrence & Rowan-Robinson (1996). The adopted aperture size is $5''$ for all ULIRGs, corresponding to ~ 5 kpc for the mean redshift. The adopted aperture is the smallest among those tabulated in Sanders et al. (1988), where the original photometric data

are taken from. Although IRAS and submm data are obtained with larger apertures, the compactness of emission source ensures negligible corrections for the aperture mismatch (Sanders et al. 1988; Wynn-Williams & Becklin 1993; Soifer et al. 2000).

For ULIRGs, galaxies with secure FUV photometry are relatively rare. Thus, we simply determine the best-fitting model for all the photometric data available. We find that our models again give a flux lower than that observed in the shorter wavelength region. We estimate f_{leak} for ULIRGs by attributing this deficiency to the photon leakage.

The best-fitting models without considering the leakage are shown in Fig. 8 with dashed lines. Our model can

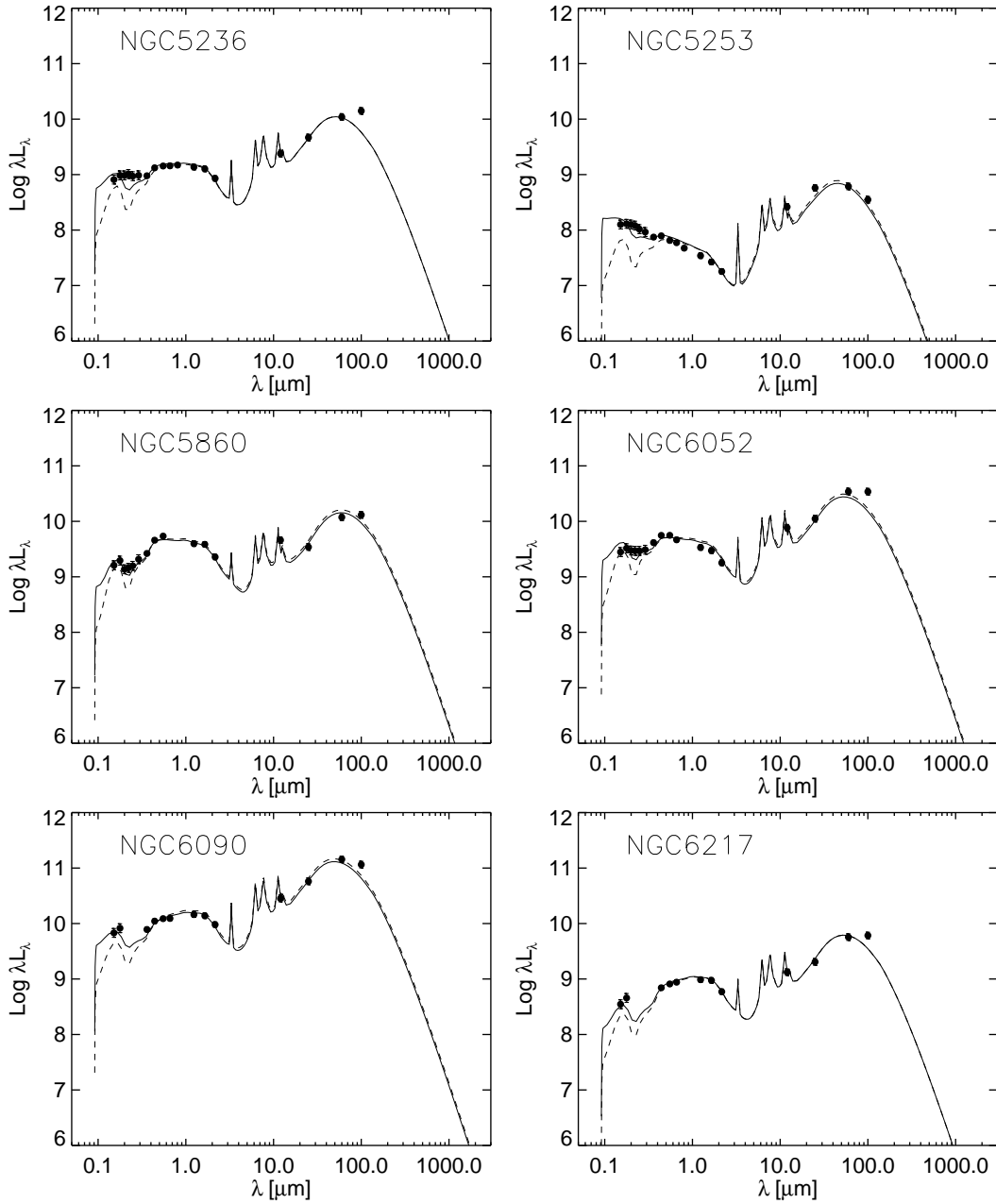


Figure 7. - continued.

reproduce the observed SEDs especially well at wavelengths longer than NIR, except for IRAS05189 and Mrk231, which are candidates for AGN powered ULIRGs. For both galaxies, it is found that the observed flux from NIR to MIR show clear excess comparing with the best-fitting model, which could be accounted for by the emission from hot dust around AGN. Thus, our fitting results are consistent with the spectroscopic classification of ULIRGs. All of starburst powered ULIRGs are best-fit with the SMC type extinction curve except for IRAS08572. This shows a clear contrast to the results for UVSBGs, in which the MW extinction curve is found to be better. All the best-fitting models are characterized by the small compactness factor $\Theta \sim 0.5$, corresponding to $\tau_V \sim 20$; as a result, the strong silicate absorption feature

at $9.7 \mu\text{m}$ is a common factor in ULIRGs. This result suggests that the starburst regions of ULIRGs are much more compact in size compared with the UVSBGs.

As already mentioned above, we can see that the best-fitting models tend to give a flux in the optical region lower than the observed one. Following our treatment of UVSBGs, we determine f_{leak} with the least square method, assuming negligible extinction for leaking photons. The best-fitting models with the leakage are shown in Fig. 8 with solid lines. The resulting fitting parameters are given in Table 2. Due to the simple assumption that the extinction is negligible for the leaking photon, the resulting SEDs in the UV are significantly bluer. Although the values of f_{leak} are smaller than those for UVSBGs, the effect of the leakage on the

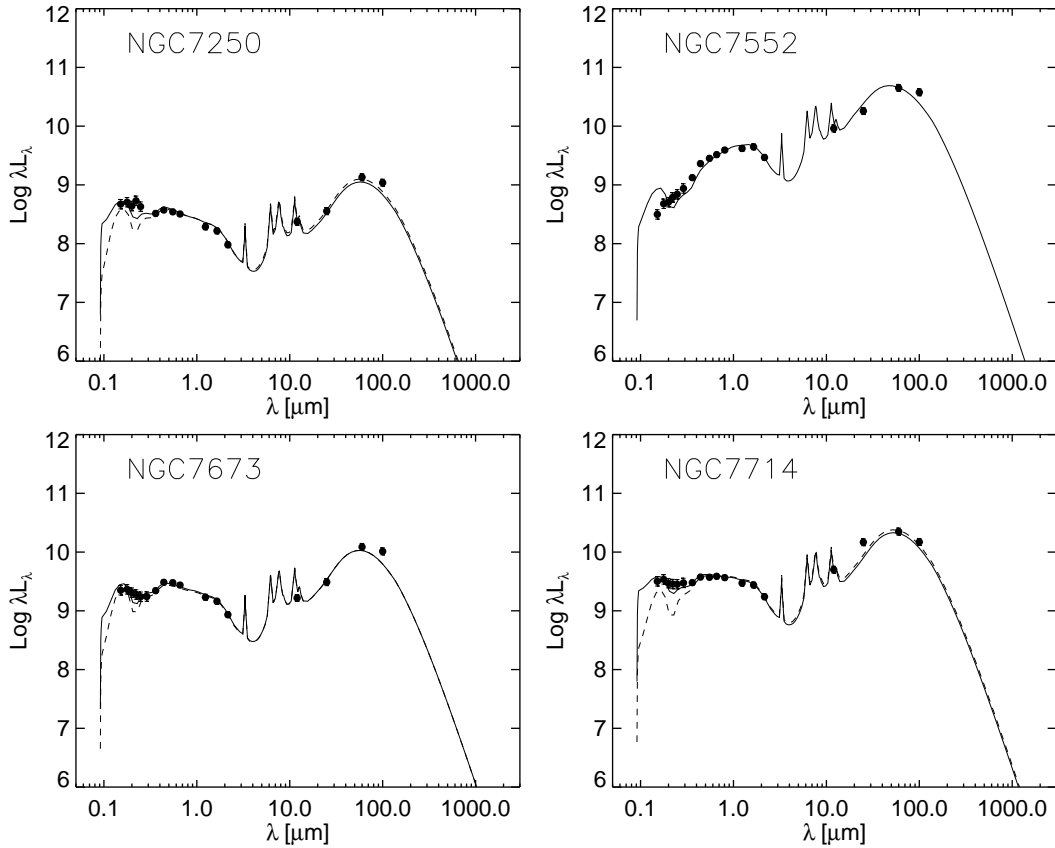
Figure 7. - *continued.*

Table 1. Fitting results for UVSBGs

name	t/t_0	Θ	EC	f_{leak}	M_T [M_\odot]	L_{bol} [L_\odot]	M_* [M_\odot]	M_D [M_\odot]	SFR [$M_\odot \text{ yr}^{-1}$]	τ_V^{eff}
IC214	4.0	0.8	MW	0.012	$2.2 \cdot 10^{10}$	$2.1 \cdot 10^{11}$	$2.0 \cdot 10^{10}$	$3.8 \cdot 10^7$	25.2	2.2
NGC1140	3.0	1.4	LMC	0.165	$3.5 \cdot 10^8$	$4.9 \cdot 10^9$	$2.7 \cdot 10^8$	$1.1 \cdot 10^6$	0.7	0.4
NGC1569	0.7	2.6	SMC	0.101	$8.9 \cdot 10^7$	$1.4 \cdot 10^9$	$1.3 \cdot 10^7$	$1.7 \cdot 10^5$	0.3	0.3
NGC1614	2.0	0.8	LMC	0.002	$1.8 \cdot 10^{10}$	$3.5 \cdot 10^{11}$	$1.0 \cdot 10^{10}$	$6.1 \cdot 10^7$	57.7	2.5
NGC4194	2.0	1.5	MW	0.004	$3.7 \cdot 10^9$	$7.1 \cdot 10^{10}$	$2.1 \cdot 10^9$	$9.1 \cdot 10^6$	11.7	1.6
NGC4385	3.0	1.3	MW	0.054	$1.1 \cdot 10^9$	$1.5 \cdot 10^{10}$	$8.1 \cdot 10^8$	$2.4 \cdot 10^6$	2.1	1.3
NGC5236	2.0	1.6	MW	0.028	$1.2 \cdot 10^9$	$2.4 \cdot 10^{10}$	$6.9 \cdot 10^8$	$3.0 \cdot 10^6$	3.9	1.2
NGC5253	0.3	2.5	MW	0.084	$2.3 \cdot 10^8$	$1.4 \cdot 10^9$	$7.9 \cdot 10^6$	$7.3 \cdot 10^4$	0.5	0.9
NGC5860	4.0	1.3	MW	0.035	$3.6 \cdot 10^9$	$3.4 \cdot 10^{10}$	$3.2 \cdot 10^9$	$6.2 \cdot 10^6$	4.1	0.9
NGC6052	2.0	1.8	MW	0.038	$3.2 \cdot 10^9$	$6.0 \cdot 10^{10}$	$1.8 \cdot 10^9$	$7.7 \cdot 10^6$	10.0	0.9
NGC6090	2.0	1.5	MW	0.017	$1.4 \cdot 10^{10}$	$2.7 \cdot 10^{11}$	$7.9 \cdot 10^9$	$3.5 \cdot 10^7$	45.0	1.5
NGC6217	3.0	1.3	MW	0.013	$9.6 \cdot 10^8$	$1.3 \cdot 10^{10}$	$7.3 \cdot 10^8$	$2.2 \cdot 10^6$	1.9	1.4
NGC7250	2.0	2.4	MW	0.088	$1.5 \cdot 10^8$	$2.8 \cdot 10^9$	$8.1 \cdot 10^7$	$3.5 \cdot 10^5$	0.4	0.5
NGC7552	2.0	1.3	MW	< 0.001	$4.6 \cdot 10^9$	$8.8 \cdot 10^{10}$	$2.6 \cdot 10^9$	$1.1 \cdot 10^7$	14.5	2.1
NGC7673	2.0	2.2	MW	0.032	$1.3 \cdot 10^9$	$2.5 \cdot 10^{10}$	$7.3 \cdot 10^8$	$3.2 \cdot 10^6$	4.1	0.6
NGC7714	2.0	1.8	MW	0.057	$2.5 \cdot 10^9$	$4.7 \cdot 10^{10}$	$1.4 \cdot 10^9$	$5.9 \cdot 10^6$	7.7	0.9

SED is prominent because of heavy obscuration of the stellar continuum. In order to verify the fitting results, we plot the FUV photometric data (Trentham et al. 1999; Goldader et al. 2002) for some of the ULIRG sample with open circles in Fig. 8. For Mrk273, IRAS08572 and IRAS12112, the FUV data taken by the *HST* are consistent with the best-fitting model without considering the leakage (dashed line),

while for IRAS15250 and IRAS22491 the FUV data can be explained by the best-fitting model with the leakage (solid line). Only for Arp220, the FUV data cannot be explained by both cases. According to Goldader et al. (2002), these data are problematic due to uncertainty of sky level, since the angular size of Arp220 is large enough to cover entire field of view of *HST*/STIS. Thus, fitting results are con-

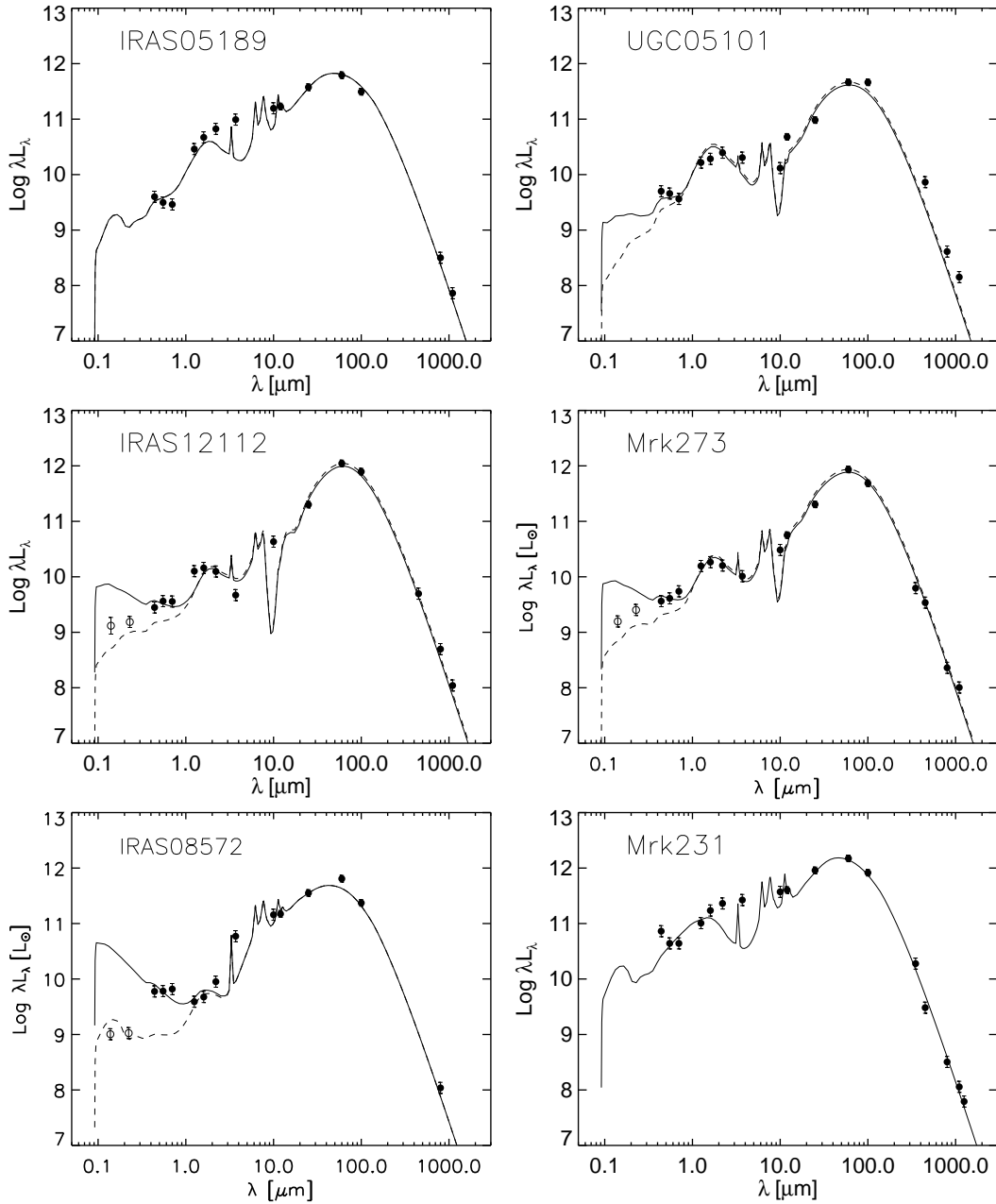


Figure 8. The same as Fig. 7, but for ultraluminous infrared galaxies. Open circles for IRAS12112, IRAS08572, IRAS15250, Arp220 and IRAS22491 indicate the photometric data, obtained by the Hubble Space Telescope (Trentham, Kormendy & Sanders 1999; Goldader et al. 2002).

sistent with FUV observations, except for the problematic case of Arp220, when we consider the derived value of f_{leak} as the upper limit for some galaxies.

As mentioned earlier, starburst ages are difficult to assign, but our resulting ages are in the range of 50–500 Myr, which shows no systematic deviation from those derived for UVSBGs. For starburst dominated ULIRGs, the mean value of Θ and τ_V^{eff} is 0.46 and 4.9, respectively. Thus, ULIRGs are more compact than UVSBGs by a factor of 3.5.

For most of the ULIRGs, the SMC extinction curve is found to provide the best fit. Note that neither the observations of silicate absorption features nor the bump at 2175 Å are used to distinguish the type of extinction curve in

the SED fitting. The SED from MIR to submm wavelengths can be better reproduced with the model in which the self-absorption of MIR emission by dust is significant; i.e., the model with the SMC extinction curve.

4.3 Comparison with emission line measurements

4.3.1 Star formation rate

In Fig. 9, we compare the resulting SFRs with the observed values derived from H α luminosities for UVSBGs (Storchi-Bergmann et al. 1994) and from the FIR luminosity of ULIRGs by using the relation presented by Kennicutt

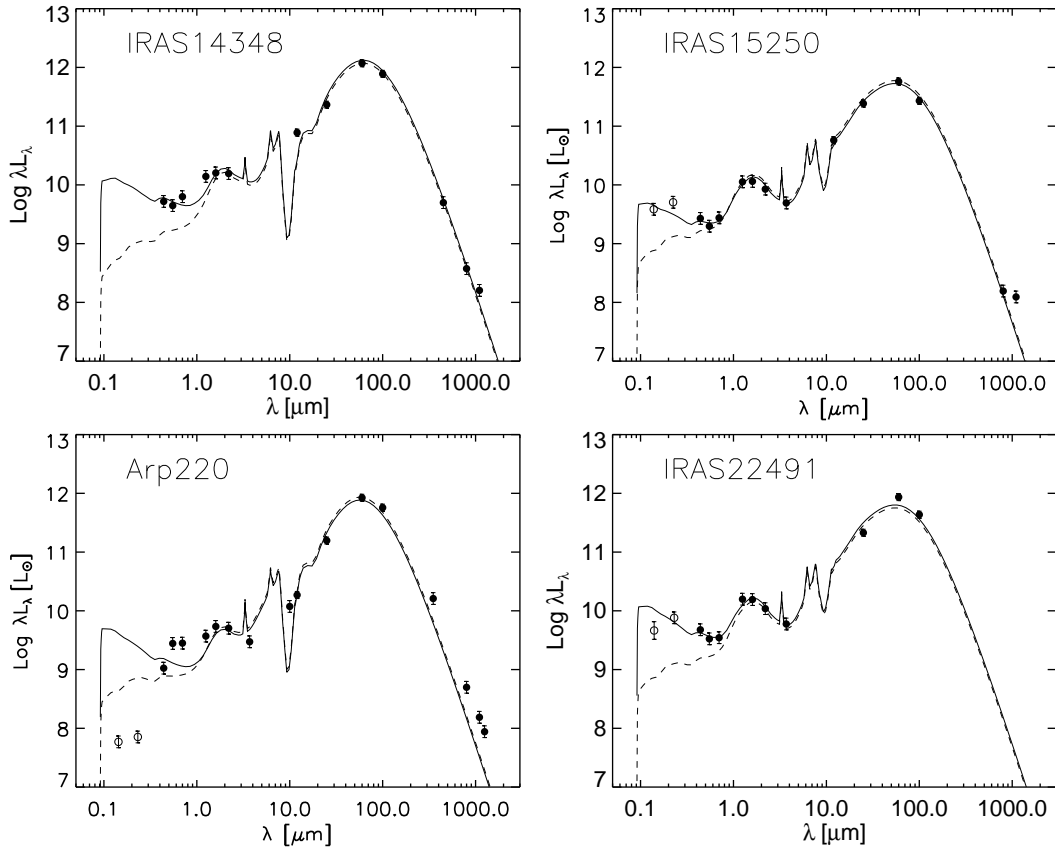
Figure 8. - *continued.*

Table 2. Fitting results for ULIRGs

name	t/t_0	Θ	EC	f_{leak}	M_T [M_\odot]	L_{bol} [L_\odot]	M_* [M_\odot]	M_D [M_\odot]	SFR [M_\odot/yr]	τ_V^{eff}
UGC05101	5.0	0.3	SMC	0.005	$1.1 \cdot 10^{11}$	$2.1 \cdot 10^{12}$	$1.0 \cdot 10^{11}$	$2.5 \cdot 10^8$	69.	4.7
IRAS12112	2.0	0.3	SMC	0.006	$7.8 \cdot 10^{10}$	$1.5 \cdot 10^{12}$	$4.3 \cdot 10^{10}$	$3.5 \cdot 10^8$	244.	5.4
Mrk273	2.0	0.4	SMC	0.008	$6.6 \cdot 10^{10}$	$1.3 \cdot 10^{12}$	$3.7 \cdot 10^{10}$	$3.0 \cdot 10^8$	207.	4.9
IRAS08572	0.5	0.8	MW	0.036	$9.2 \cdot 10^{10}$	$1.7 \cdot 10^{12}$	$7.7 \cdot 10^9$	$6.0 \cdot 10^7$	285.	4.9
IRAS14348	2.0	0.3	SMC	0.008	$1.0 \cdot 10^{11}$	$2.0 \cdot 10^{12}$	$5.8 \cdot 10^{10}$	$4.8 \cdot 10^8$	327.	5.4
IRAS15250	1.0	0.6	SMC	0.005	$4.8 \cdot 10^{10}$	$9.1 \cdot 10^{11}$	$1.2 \cdot 10^{10}$	$1.4 \cdot 10^8$	185.	4.5
Arp220	0.7	0.4	SMC	0.004	$7.2 \cdot 10^{10}$	$1.4 \cdot 10^{12}$	$1.0 \cdot 10^{10}$	$1.4 \cdot 10^8$	260.	5.4
IRAS22491	1.0	0.6	SMC	0.011	$5.7 \cdot 10^{10}$	$1.1 \cdot 10^{12}$	$1.4 \cdot 10^{10}$	$1.6 \cdot 10^8$	221.	4.4
IRAS05189 ^a	4.0	0.4	MW	< 0.001	$1.4 \cdot 10^{11}$	$2.7 \cdot 10^{12}$	$1.2 \cdot 10^{11}$	$2.4 \cdot 10^8$	158.	4.7
Mrk231 ^a	2.0	1.0	MW	< 0.001	$1.6 \cdot 10^{11}$	$3.1 \cdot 10^{12}$	$8.9 \cdot 10^{10}$	$3.9 \cdot 10^8$	506.	2.8

Note: ^a candidates for AGN powered ULIRGs

(1998). The SFRs in our model are basically determined from the bolometric luminosity from UV to FIR. Therefore, the observed SFRs for ULIRGs should be almost identical to those from the SED fitting since the emission from the FIR dominates the SED of ULIRGs. Thus, we can see clearly this agreement at the high SFRs. On the other hand, our SFR derivation is independent of that from H α line emission for UVSBGs. Although the difference between the model results and observation becomes large for galaxies with the SFR $\leq 1 M_\odot \text{ yr}^{-1}$, the resulting SFRs for UVSBGs agree well with those derived from H α and IR luminosities over three orders of magnitude without any systematic difference. Therefore,

the SFR estimated by the SED fitting can be applied well to any starburst galaxy regardless of their optical depth.

Our SED model suggests that leaking photons contribute to the UV luminosities of starbursts. Therefore, if the UV luminosity is corrected for dust extinction without considering this contribution, the UV-derived SFR can be easily overestimated. This effect may explain the excess of UV luminosities for a given H α luminosity, reported by Sullivan et al. (2000). We emphasize that, in order to derive SFRs from the continuum emission, bolometric luminosity should be used to avoid systematic effects.

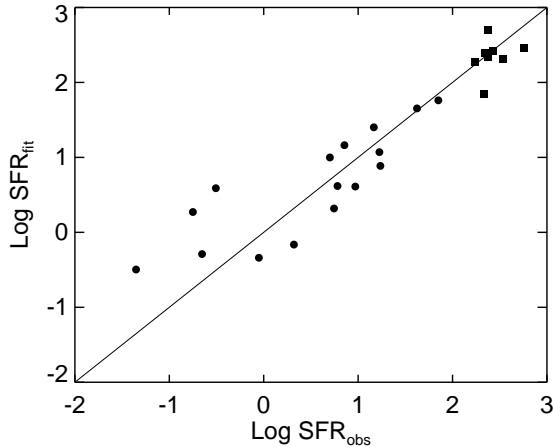


Figure 9. Comparison of the SFR in $M_{\odot}\text{yr}^{-1}$. The observed SFRs are derived from the extinction corrected $H\alpha$ and FIR luminosity for UVSBGs and ULIRGs, respectively. AGN candidates, IRAS05189 and Mrk231, are not plotted. Solid line indicates the linear relation.

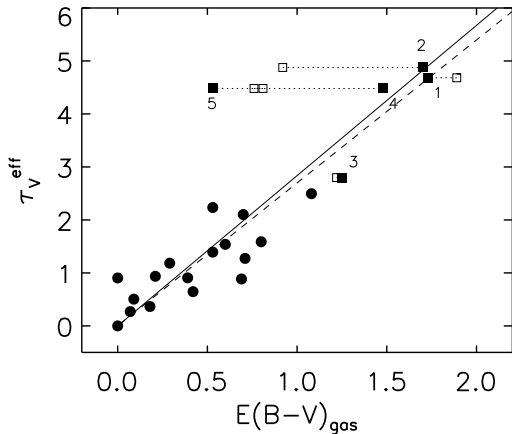


Figure 10. Comparison of the extinction. The observed colour excesses $E(B - V)_{\text{gas}}$ are derived from the ratios of emission lines. For UVSBGs, $H\alpha/H\beta$ is used, taken from Storchi-Bergmann et al. (1994). For ULIRGs, only galaxies which have observed value of $\text{Pa}\alpha$ are plotted; depicted numbers indicate galaxies; 1 - IRAS08572, 2 - IRAS12112, 3 - Mrk273, 4 - IRAS15250, 5 - IRAS22491. Filled and open squares indicate $E(B - V)_{\text{gas}}$ derived from $\text{Pa}\alpha/H\alpha$ and $H\alpha/H\beta$, respectively (Veilleux et al. 1999b). Solid and dashed line indicate the relation for the ratio of total-to-selective extinction $A_V/E(B - V) = 3.08$ for MW and 2.93 for SMC (Pei 1992), respectively. The derived relation between τ_V^{eff} and $E(B - V)_{\text{gas}}$ should be similar to this relation in the case that the distribution of ionized gas is the same as that of stars.

4.3.2 Optical depth and extinction

The effective optical depth can be determined independently of the SFR. In Fig. 10, we compare the effective optical depth at V-band τ_V^{eff} with the colour excess $E(B - V)_{\text{gas}}$ derived from the Balmer line ratios. We see that τ_V^{eff} is consistent with $E(B - V)_{\text{gas}}$. Calzetti et al. (1994) suggested that the

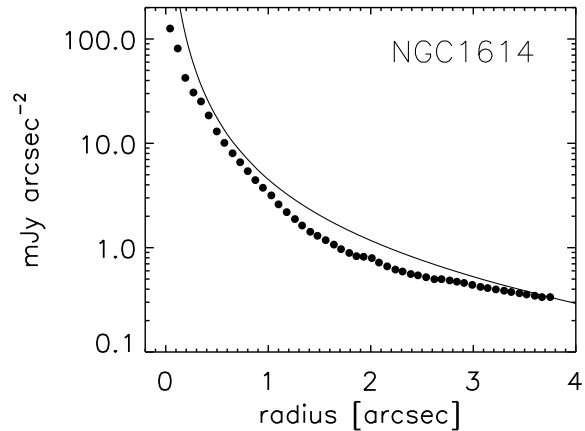


Figure 11. Comparison of K-band surface brightness profile of NGC1614. Data plotted are taken from Alonso-Herrero et al. (2001) obtained with the *HST*/NICMOS. Solid line is the surface brightness of the best-fitting SED model for NGC1614.

extinction inferred from the line ratios in starburst galaxies is typically twice as high as that derived from the stellar continuum. For optically thick UVSBGs in our sample, the resulting τ_V^{eff} tends to be slightly less (within a factor of 2) than the expected value for the MW extinction curve and therefore, consistent with the results of Calzetti et al. (1994).

The observed colour excesses $E(B - V)_{\text{gas}}$ of ULIRGs should be derived from the less attenuated lines, such as Paschen and Brackett lines, since the Balmer line ratios could be saturated due to the large optical depth. Veilleux et al. (1999b) presented $E(B - V)_{\text{gas}}$ measurements derived from both $\text{Pa}\alpha/H\alpha$ and $H\alpha/H\beta$. Both are plotted in Fig. 10, connected with dotted lines for each galaxy. Half of our sample of galaxies have the observed $\text{Pa}\alpha/H\alpha$. Except for IRAS22491, τ_V^{eff} of the ULIRG sample are consistent with the simply extrapolated relation from the less attenuated UVSBGs. For IRAS22491 (the only HII galaxy in our sample), $E(B - V)_{\text{gas}}$ derived from $\text{Pa}\alpha/H\alpha$ and $H\alpha/H\beta$ differs in the opposite sense. Galaxies showing such anomalous behaviour are predominantly Seyfert 2 galaxies in the sample studied by Veilleux et al (1999b), and HII galaxies constitute only a small fraction. The extinction of ULIRGs could be investigated more accurately by spectroscopic studies at longer wavelengths with higher sensitivity, by future FIR satellite missions, such as SIRTf and ASTRO-F.

In summary, the SED fitting model can reproduce well the relation between $E(B - V)_{\text{gas}}$ and τ_V^{eff} , and therefore, the dimming and reddening effects of the light from starburst regions are consistently introduced in the model.

4.4 Comparison of apparent effective radius

Since we applied the model not to a whole galaxy, but to the central starburst region, the effective radius derived from the SED fitting should be compared with that of the central starburst region. For the UVSBG sample, unfortunately no homogeneous presentation of effective radii of starburst regions is found in the literature. Prugniel & Heraudeau (1998) presented a catalogue of aperture photometry of 7744 galax-

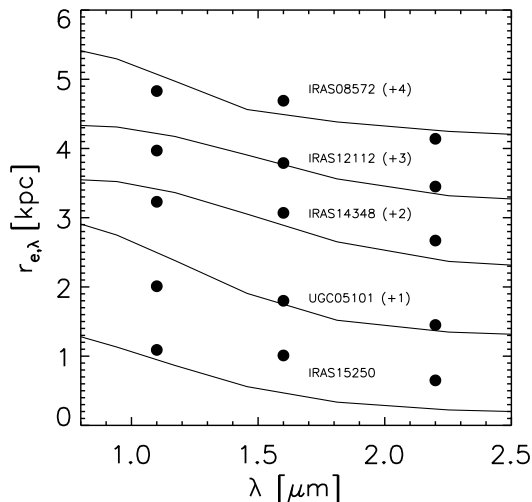


Figure 12. Comparison of the apparent effective radii at $1.1\mu\text{m}$, $1.6\mu\text{m}$ and $2.2\mu\text{m}$ with the *HST* observations (Scoville et al. 2000; solid circles) for galaxies in which the effective radius is determined for a single nucleus (see text in detail). For clarity, we add the value noted in parenthesis to the effective radii.

ies and derived B -band effective radii for a whole galaxy, including all our sample UVSBGs, but three. Note that these effective radii cannot be compared with the model results directly, since the underlying population could enlarge the B -band effective radii, systematically. It is found that B -band effective radii published by Prugniel & Heraudeau (1998) are systematically larger than those derived from the SED fitting by a factor of three. However, it is not yet clear whether the contribution from underlying population is enough to explain this discrepancy or not. This discrepancy may be partly due to the adopted concentration parameter c being too large for UVSBGs. Alonso-Herrero et al. (2001) studied NGC1614 in detail with *HST*/NICMOS observations, and presented a surface brightness profile of the central starburst region in the K -band. We compare the K -band surface brightness profile of NGC1614 with that of the best-fitting SED model in Fig. 11. Clearly, the model result is in good agreement with the observation. Since this galaxy is relatively luminous and obscured for a typical UVSBG, we need a more comprehensive study using images with high spatial resolution to confirm the stellar distribution of UVSBGs unambiguously.

Scoville et al. (2000) presented NIR images of ULIRGs obtained with the *HST*/NICMOS, and derived the effective radii at $1.1\mu\text{m}$, $1.6\mu\text{m}$ and $2.2\mu\text{m}$. In most cases, the observed effective radii are less than $1''$, and are therefore consistent with the adopted aperture size as starburst regions ($5''$) in the SED fitting. We focus on the ULIRGs for which the effective radii are determined for isolated major starburst regions, since the multiple structure could enlarge the effective radius, systematically. In Fig. 12, the effective radii of the models for ULIRGs are compared with the apparent effective radii from the *HST*/NICMOS images. As a result, we can see that the radii from the models and the observations are consistent with each other within a factor of 2. As

shown in the Fig. 12, the effective radius of isolated starburst region in the K -band is < 0.7 kpc, which corresponds to an intrinsic effective radius (i.e., for the case without dust) of ~ 0.3 kpc. Scoville et al. (2000) have shown that the light profiles of these ULIRGs can be also fitted well with the $r^{1/4}$ law, which can be reproduced by the King profile. Thus, the stellar distribution in a starburst region can be roughly represented with our model geometry of the King profile with $\log(r_t/r_c) = 2.2$ for ULIRGs.

As shown by Scoville et al. (2000), many ULIRGs have multiple starburst regions – such as Arp 220. As long as each starburst region has a constant surface brightness, the SED feature is not affected by this multiplicity as remarked in the model description (Section 2.2). Thus, the model geometry can still work as long as the stellar distribution of individual starburst regions are considered.

4.5 Correlations between starburst properties: signature of bimodality

In Fig. 13a, the SFR is plotted against τ_V^{eff} and τ_V . Clearly, we can see a power-law correlation between SFR and τ_V^{eff} ; $\text{SFR} \propto (\tau_V^{\text{eff}})^3$. A similar trend has already been shown by Heckman et al. (1998) and Adelberger & Steidel (2000) between $L_{\text{FIR}}/L_{\text{UV}}$ and $L_{\text{UV}+\text{FIR}}$, which are related to the reddening effects and SFR respectively, although the dispersion of the correlation they presented was much larger than that shown in Fig. 13a. This trend seems to suggest the Schmidt law for star formation, in which SFR increases with increasing gas density. However, note that not τ_V^{eff} , but τ_V is proportional to the gas column density in the starburst regions. The discrepancy between τ_V^{eff} and τ_V can be clearly seen at high optical depth $\tau_V \gtrsim 5$; as a result, the SFR seems to saturate at $\tau_V \gtrsim 5$. This suggests that the mode of starburst activity changes at a critical column density corresponding to $\tau_V \simeq 5$.

Such bimodal feature can be seen in the relation between the SFR and the compactness factor as shown in Fig. 13b, in which we can also find a critical compactness factor $\Theta^{-2} \simeq 3$. Both bimodal features of the SFR against the column density and the compactness suggest that the gas density in the starburst regions can directly affect the starburst activity since in general the geometrical compactness with the high column density implies the existence of a high density region.

In Fig. 13c, we plot f_{leak} against τ_V^{eff} and τ_V . There is an anti-correlation between these properties for $\tau_V \lesssim 5$, while this anti-correlation breaks for larger τ_V . Feedback in starbursts with low ISM density, such as UVSBGs, may naturally generate regions of porous ISM that provide pathways for UV photon leakage even from central region of starbursts. On the other hand, for starbursts with a high density ISM such as ULIRGs, leakage can be expected only from the outermost surface of a starburst region and may have little to do with the main starburst (Goldader et al. 2002). Thus, the break of anti-correlation between f_{leak} and τ_V can be explained by the feedback effects on different ISM density.

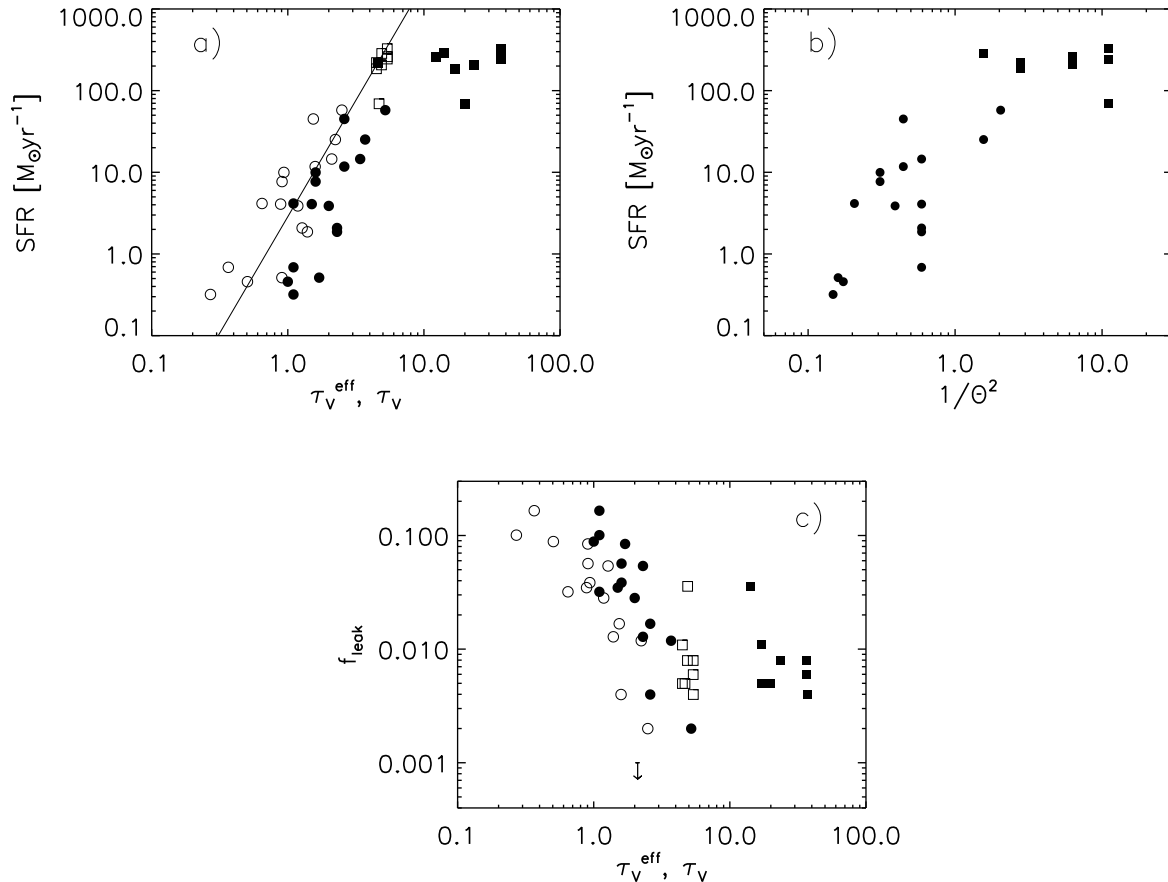


Figure 13. Relations between the derived quantities. Circles and squares indicate UVSBGs and ULIRGs, respectively. a) SFRs are plotted against the effective V -band optical depth (open symbols) and V -band optical depth (solid symbols). The solid line is a power-law relation, $\text{SFR} \propto (\tau_V^{\text{eff}})^3$. b) SFRs are plotted against Θ^{-2} , which is proportional to τ_V for constant dust mass. c) Leaking fraction as a function of τ_V^{eff} (open symbols) and τ_V (solid symbols). Upper limit on f_{leak} is indicated with an arrow.

5 DISCUSSION

In this section, we will discuss the bimodality found in the correlations between starburst properties with our SED diagnostics. First, we focus on the correlation between the intrinsic surface brightness and the size of starburst region, which shows the bimodality with a clear limit on the size of starburst regions. Then, we investigate the origin of the bimodality in the starburst activity by considering the physical processes of starburst regions, such as gravitational instability of the disc and feedback effects.

5.1 Bimodal starburst intensity

In Fig. 14, the bolometric luminosities of starburst galaxies are plotted against the effective radii. Filled circles and squares are bolometric luminosities and intrinsic effective radii (i.e., for the case without dust) derived from the SED model of UVSBGs and ULIRGs, respectively. The bolometric surface brightnesses of UVSBGs are found to be almost constant at $10^{12} L_{\odot} \text{kpc}^{-2}$. On the other hand, a clear limit on the intrinsic effective radius can be seen at ~ 0.3 kpc. Moreover, the bolometric surface brightnesses of ULIRGs

are an order of magnitude higher than those of UVSBGs. This suggests that the mode of starbursts could change at $L_{\text{bol}} \simeq 10^{11} L_{\odot}$ and $r_e \simeq 0.3$ kpc.

A limiting bolometric starburst intensity $L_{\text{bol}} r_e^{-2} = 2 \times 10^{11} L_{\odot} \text{kpc}^{-2}$ was proposed by Meurer et al. (1997). From this intensity limit, they also proposed a global star formation limit $\psi r_e^{-2} \simeq 45 M_{\odot} \text{kpc}^{-2} \text{yr}^{-1}$. In Fig. 14, all open symbols other than open squares indicate the original data used by Meurer et al. (1997). For open squares, we adopt the effective radii of ULIRGs observed with the *HST*/NICMOS at $2.2 \mu\text{m}$ taken from Scoville et al. (2000). These effective radii are systematically smaller than those derived from R -band images (Lehnert & Heckman 1996; small open diamonds) and from images of $\text{H}\alpha$ emission (Armus et al. 1990; small open triangles), although the similar class of galaxies is investigated. Thus, from the observational results it is suggested that the observed surface brightness depends on the observed wavelength. For UVSBGs, the bolometric surface brightness calculated with the intrinsic effective radius is higher by a factor of 5 than the proposed value by Meurer et al. (1997). The difference between the intrinsic and observed surface brightness is more remarkable for ULIRGs and indicates a bimodal starburst activity.

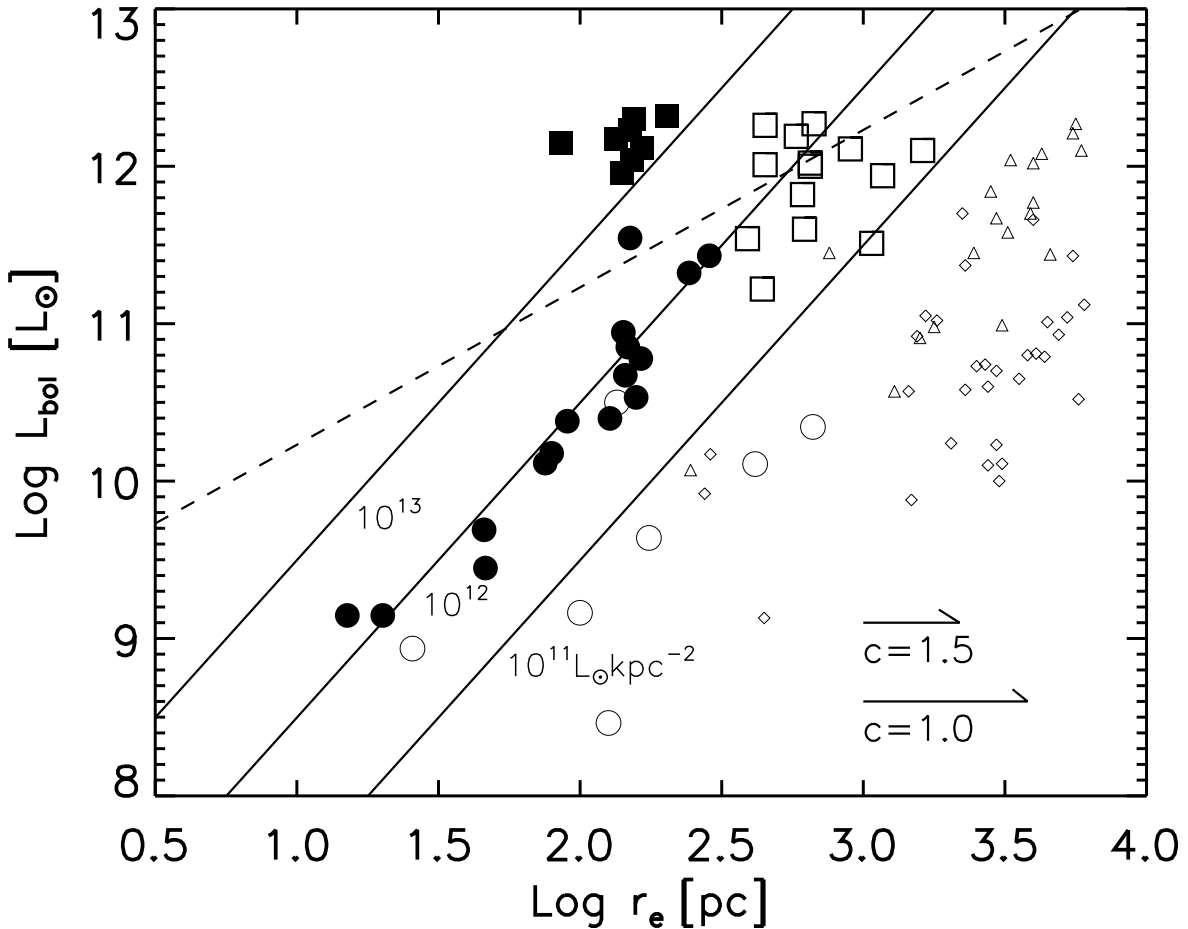


Figure 14. The bolometric luminosities of starburst galaxies plotted against effective radii. Filled circles and squares are the bolometric luminosities and intrinsic effective radii derived from the SED of UVSBGs and ULIRGs, respectively. Open symbols indicate the observed bolometric luminosities and apparent effective radii at $0.22\mu\text{m}$ (open circles; Meurer et al. 1995), $2.2\mu\text{m}$ (squares; Scoville et al. 2000). Small diamonds indicate the R -band effective radii and L_{bol} taken from Lehnert & Heckman (1996) in which L_{bol} is estimated from FIR luminosity ($L_{bol} = 1.5L_{FIR}$; Meurer et al. 1997). When R -band data is not available, we convert the effective radius measured with $H\alpha$ imaging into R -band effective radius with the average ratio of $H\alpha$ to R -band effective radius, 0.6 according to Lehnert & Heckman (1996). By using the same ratio of effective radii, $H\alpha$ effective radii taken from Armus et al. (1990) are converted to R -band effective radii, which are plotted against L_{bol} estimated again from L_{FIR} (small triangles). Dashed line is the limiting luminosity given in Eq. (21). Two arrows at the bottom left corner indicate the effect of concentration parameter c on the resulting r_e .

Actually, the limit on bolometric surface brightness we derive depends on the precise value of adopted concentration parameter c . In Fig. 14, we adopt $c = 2.2$ for all cases. As discussed in Section 4.4, it is possible that this concentration parameter could be large for UVSBGs. In Fig. 14, we show the correction factor for the intrinsic effective radius in the case of $c=1.0$ and 1.5 by arrows at the bottom left corner. Nevertheless, the derived limit on the surface brightness is robust for active starburst galaxies, since we confirmed in Section 4.4 that for ULIRGs and relatively luminous UVSBGs the adopted value $c=2.2$ is reasonably consistent with observed effective radii. Note that even if less active starbursts have the smaller value of concentration parameter, the bimodal feature of starburst activity shown in Fig. 14 still remains.

In summary, the SED diagnostics find that 1) UVSBGs have an intrinsic effective surface brightness $L_{bol}r_e^{-2} \simeq 10^{12} L_{\odot}\text{kpc}^{-2}$, and 2) there is a limit on the size of the starburst region of around 0.3 kpc. Considering these results, we will propose a picture of bimodal starburst activity which consists of mild starburst activity in UVSBGs with a regulated surface intensity around $L_{bol}r_e^{-2} \simeq 10^{12} L_{\odot}\text{kpc}^{-2}$ and an intensive mode of starbursts in ULIRGs confined in the region of $r_e \simeq 0.3$ kpc. In the next subsection, we will discuss the physical origin of this bimodality.

5.2 Origin of bimodal starbursts

5.2.1 Disc instability in UVSBGs

The regulating mechanisms for the mild starburst intensity have already been proposed by Meurer et al. (1997). Following Kennicutt (1989), they showed that the gas surface density is somewhat close to a critical value at which gas discs would be unstable to self-gravity. According to Toomre (1964) and Quirk (1972), Kennicutt (1989) proposed the critical surface density for inducing star formation with the instability is

$$\Sigma_c = \frac{\alpha \kappa \sigma_g}{\pi G}, \quad (14)$$

where σ_g is the velocity dispersion of the gas and κ is the epicyclic frequency. The parameter α is a constant empirically determined as $\simeq 0.63$. With angular frequency $\Omega(r) = V(r)/r$, the epicyclic frequency is given by

$$\kappa = \left(r \frac{d\Omega^2}{dr} + 4\Omega^2 \right)^{1/2}. \quad (15)$$

While Kennicutt (1989) considered the instability around the flat part of the rotation curve in disc galaxies, Meurer et al. (1997) applied it for the nuclear starbursts near the peak of the rotation curve in inner discs. We also apply the technique of Meurer et al. to interpret the bimodal trends of SFRs in Fig. 14. If we consider that the inner disc to be a rigid rotator with a angular frequency Ω , the dynamical time of the disc is given by

$$t_{dyn} = \frac{\pi}{2\Omega}. \quad (16)$$

With a constant Ω for the inner disc, the critical surface density is $\Sigma_c = 2\alpha\sigma\Omega/(\pi G)$. With the estimations for the dynamical time and the surface density, the maximum star formation intensity can be expected as

$$\dot{\Sigma}_* \simeq \frac{\Sigma_c}{t_{dyn}} = 9 \times 10^{-5} \alpha \sigma \Omega^2 \text{ M}_\odot \text{ yr}^{-1} \text{ kpc}^{-2}, \quad (17)$$

where σ and Ω are in units of km s^{-1} and $\text{km s}^{-1} \text{ kpc}^{-1}$, respectively.

With $\psi(t)/L_{bol}$ from Eq. (11), the bolometric surface brightness limit can be introduced as

$$\begin{aligned} L_{bol} r_e^{-2} &\simeq 3.1 \times 10^5 \alpha \sigma \Omega^2 \text{ L}_\odot \text{ kpc}^{-2} \\ &= 3.7 \times 10^{12} \left(\frac{\alpha}{0.61} \right) \left(\frac{\sigma}{20 \text{ km s}^{-1}} \right) \\ &\quad \times \left(\frac{\Omega}{10^3 \text{ km s}^{-1} \text{ kpc}^{-1}} \right)^2 \text{ L}_\odot \text{ kpc}^{-2}, \end{aligned} \quad (18)$$

where we take $t/t_0 = 2$ as a typical observable starburst age.

Since most of disc galaxies have a central HI velocity dispersion $\sigma_g \simeq 15 - 20 \text{ km s}^{-1}$ (e.g. Dickey, Hanson & Helou 1990) and angular frequency $\Omega < 10^3 \text{ km s}^{-1} \text{ kpc}^{-1}$ (e.g. Armus et al. 1990), this limiting bolometric surface brightness ($\sim 3.7 \times 10^{12} \text{ L}_\odot \text{ kpc}^{-2}$) corresponds well to the limiting intensity of UVSBGs as seen in Fig. 14. Thus, starbursts in UVSBGs can be triggered by the self-gravitational instability in inner gas discs as already pointed out by Meurer et al. (1997). This instability seems to induce only mild starburst activity, since the unstable region should have a scale of the disc thickness, and the whole gas in the disc cannot concentrate into the unstable region due to the centrifugal

Table 3. Velocity dispersions of starburst galaxies

name	σ [km/sec]	Line ^a
UBSBGs		
IC214	124.6	HI [21cm]
NGC1140	62.3	HI [21cm]
NGC1569	23.1	HI [21cm]
NGC1614	75.0	CO 2.3 μ m
NGC1614	107.7	CO(1 \rightarrow 2)
NGC4194	41.7	HI [21cm]
NGC4194	104.0	CO 2.3 μ m
NGC4194	73.2	CO(1 \rightarrow 2)
NGC4385	36.7	HI [21cm]
NGC5236	78.2	HI [21cm]
NGC5253	25.8	HI [21cm]
NGC6052	127.8	HI [21cm]
NGC6090	61.4	HI [21cm]
NGC6090	50.0	CO 2.3 μ m
NGC6090	55.2	CO(1 \rightarrow 2)
NGC6217	61.6	HI [21cm]
NGC7250	52.0	HI [21cm]
NGC7552	62.9	HI [21cm]
NGC7673	51.1	HI [21cm]
NGC7714	65.0	HI [21cm]
NGC7714	106.6	CO(1 \rightarrow 2)
ULIRGs		
IRAS12112	146.4	CO(1 \rightarrow 2)
Mrk273	71.8	CO(1 \rightarrow 2)
Mrk273	160.0	CO 2.3 μ m
IRAS14348	107.7	CO(1 \rightarrow 2)
Arp220	182.3	CO(1 \rightarrow 2)
Arp220	150.0	CO 2.3 μ m
IRAS22491	85.6	CO(1 \rightarrow 2)

Note: ^a Emission lines (HI 21cm; CO(1 \rightarrow 2)) and absorption line (CO 2.3 μ m) adopted to derive the velocity dispersion. See the caption of Fig. 15 for references to the observations.

force from the disc's rotation. This means that the maximum size of starburst regions is expected to be similar to the disc thickness $\sim 0.3 \text{ kpc}$, and therefore consistent with the SED fitting results in which no starbursts with $r_e \gtrsim 0.3 \text{ kpc}$ are found.

The surface brightness of ULIRGs are an order of magnitude larger than that expected from the disc instability. Therefore, ULIRGs should be triggered by another mechanism which can induce a stronger concentration of gas. As indicated by Eq. (18), the surface brightness of starburst regions in UVSBGs are related to the physical properties of parent galaxies. On the other hand, the strong mass concentration in the central region of ULIRGs should result in the strong self-gravity of starburst region, and therefore the starburst region in ULIRGs can be dynamically isolated from parent galaxies. In such a case, the surface brightness of ULIRGs should be controlled by the relative strength of the self-gravity and its feedback.

5.2.2 Self-gravity vs. feedback in ULIRGs

For a starburst with a typical duration of t_0 , the kinetic energy of gas clouds with random velocity v_g can be written as $1/2 M_g v_g^2 \simeq L_{kin} t_0$, where L_{kin} is the kinetic luminosity due to feedback. Assuming that L_{kin} is proportional to the

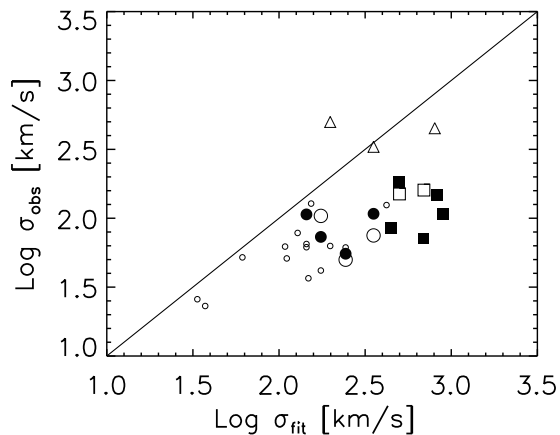


Figure 15. Comparison of velocity dispersions in starburst regions. We estimate the velocity dispersions from the SED fitting results; i.e., $\sigma_{fit} = (GM(< r_e)/2r_e)^{1/2}$ where we assume $M(< r_e) = 2M_*(< r_e)$. Squares and circles indicate ULIRGs and UVSBGs, respectively. For solid symbols, we adopt the velocity dispersions derived from the line profile of the CO(1→2) emission (Sanders, Scoville & Soifer 1991), while HI line width measurements are used for small open circles, which are taken from LEDA database. To convert both CO and HI line widths to the velocity dispersion, we assume that the line profile is Gaussian; i.e., $\sigma = \text{FWHM}/2.35 = W_{20}/3.62$, where W_{20} is the width at 20% of the peak. For large open circles and open squares, we adopt velocity dispersions derived from the $2.3 \mu\text{m}$ CO absorption feature (James et al. 1999; Shier & Fischer 1998). For open triangles, we plot terminal velocities, instead of velocity dispersions, which are obtained for Mrk273 (450 km s^{-1}), NGC1614 (330 km s^{-1}) and NGC7552 (500 km s^{-1}) by Heckman et al. (2000).

bolometric luminosity with a constant efficiency f_{kin} , i.e., $L_{kin} = f_{kin}L_{bol}$, we can write the kinetic energy per a unit mass as

$$\frac{1}{2}v_g^2 = \frac{L_{kin}t_{dyn}}{M_g} = f_{kin} \frac{L_{bol}}{\psi}. \quad (19)$$

By using the relation between L_{bol} and SFR ψ in Eq. (11), the typical velocity can be written as

$$v_g = 454 \left(\frac{f_{kin}}{0.01} \right)^{1/2} \left(\frac{t}{t_0} \right)^{1/2} \text{ km s}^{-1}. \quad (20)$$

Note that the effect of feedback is independent of the mass in the starburst regions and also in the host galaxies, even though a larger gas supply can induce a more active starburst. On the other hand, the gravitational effect becomes more prominent in more massive systems. This means that too massive starbursts cannot be sustained by feedback against strong self-gravity.

This limiting effect of feedback against self-gravity can be estimated by the comparison of v_g with the escape velocity $v_{esc,c}$ ($v_{esc,c}^2 \simeq 2GM(< r_e)r_e^{-1}$), which indicates the depth of the gravitational potential well. A critical mass-radius relation is expected for the condition, $v_{esc,c} = v_g$. This relation can be rewritten to another luminosity-radius relation by using the mass to light ratio of starburst regions [Eq. (12)]. We can then introduce a limiting bolometric lu-

minosity

$$\begin{aligned} L_{bol,c} &\simeq 1.2 \times 10^2 \left(\frac{M_*}{M_\odot} \right) \left(\frac{t}{t_0} \right)^{-1.8} L_\odot \\ &\simeq 1.5 \times 10^{12} \left(\frac{f_{kin}}{0.01} \right) \left(\frac{M_*}{M_*(< r_e)} \right) \\ &\quad \times \left(\frac{r_e}{1 \text{ kpc}} \right) \left(\frac{t}{t_0} \right)^{-0.8} L_\odot, \end{aligned} \quad (21)$$

for $t_0 = 100 \text{ Myr}$, where we use $M(< r_e) = 2M_*(< r_e)$. The total mass within r_e is somewhat uncertain, since a realistic distribution of gas and the contribution from the dark matter is important. Therefore, we simply assume $M(< r_e) = 2M_*(< r_e)$. At a typical starburst stage $t/t_0 = 2$, we take a limiting bolometric luminosity $L_{bol,c} \simeq 1.7 \times 10^{12} (r_e/1 \text{ kpc}) L_\odot$. The feedback effect cannot sustain the starburst region against self-gravity when the bolometric luminosity exceeds this limit. This limiting luminosity is indicated by the dashed line in Fig. 14, which crosses the line of limiting luminosity of the starbursts induced by the disc instability around 0.3 kpc. Fig. 14 shows that all the ULIRGs are above the dashed line where the feedback effect cannot sustain the starburst region against the self-gravity, while all the UVSBGs but one are below the dashed line. Therefore, the mode of starburst in ULIRGs can be different from that in UVSBGs as expected.

The SED diagnostics for ULIRGs indicate a strong mass concentration in the starburst regions as shown in Fig. 13 b). Furthermore, the analysis of self-gravity and feedback allow us to specify that starburst regions in ULIRGs are too massive to be sustained by the feedback effect. Such a system in ULIRGs should be dynamically unstable, which can be confirmed by the observed kinematical signature. With the mass and effective radius derived from the SED fitting, we can estimate the velocity dispersion as $\sigma_{fit} = (GM(< r_e)/2r_e)^{1/2}$, which is independent of the direct kinematical estimation from line observations. If a starburst region is dynamically stable as a virialized system, the observed velocity dispersion should be close to this value. In Fig. 15, we compare σ_{fit} with observed velocity dispersions. The observed velocity dispersions are derived from the emission lines of CO(1→2) and HI at 21cm, and the absorption line of CO at $2.3 \mu\text{m}$. These velocity dispersions are tabulated in Table 3. The velocity dispersions by $2.3 \mu\text{m}$ CO absorption are most suitable to probe the gravitational potential in the starburst region, since the effect of bulk motion on the CO absorption feature is less important than that on gas emission lines. Comparing to the HI 21 cm lines, the emission line of CO molecules seems to be more suitable for our purpose, since these molecules are more concentrated in the starburst region in general. However, we also rely on the measurements of HI 21cm line, since the observation of this line can be found in the majority of our sample galaxies, and HI line widths correlate well with the other kinematical tracers such as H α and O[II] which are strong in the starburst region (Kobulnicky & Gebhardt 2000). Note that cool gas is kinematically decoupled with the outflowing gas which is indicated by triangles in Fig. 15.

We can see in Fig. 15 that the sequence of the velocity dispersion seems to be bimodal, again. The deviation of the observed velocity dispersion is most remarkable for ULIRGs. This means that, for ULIRGs, the whole starburst

region is dynamically unstable since the observed velocity dispersion is not enough to support it against the gravity due to large masses derived from the SED diagnostics. Such a dynamically unstable state for ULIRGs cannot be caused by the local disc instability as in UVSBGs, since it requires large mass concentration into the whole starburst region. Therefore, the dynamical disturbance of a galactic scale is necessary to activate ULIRGs. The merging of galaxies can be the most plausible trigger mechanism of ULIRGs.

6 CONCLUSIONS

We develop an evolutionary SED model of starburst regions in which the stellar and chemical evolution, including dust, are taken into account consistently. We investigate the basic properties of nearby starburst galaxies, such as the SFR, optical depth and apparent effective radius by using this evolutionary SED model. We studied the SED of various starburst galaxies with a SFR of $0.5 - 300 M_{\odot} \text{ yr}^{-1}$, classified as UVSBGs or ULIRGs. Our SED model essentially reproduces all the SEDs of analysed starburst galaxies over the whole range of starburst activity. For starburst galaxies having AGN, we find a clear excess of MIR emission when compared with the best-fitting SED model. The fitting results are confirmed by comparing the derived SFRs and optical depths with the emission line measurements. Irrespective of the degree of reddening, our model can derive the SFR of starburst regions in a unified manner. The apparent effective radii derived from the SED fitting are found to be consistent with observations. Thus, our model can derive both the SFR and intrinsic effective radius from the SEDs.

The variety of the starburst SEDs is caused mainly by the compactness of starburst regions, not from the starburst age. From the SED diagnostics, we find bimodal correlations between the SFR and the compactness/optical depth; more active starburst regions tend to be more compact and heavily obscured.

The bimodal starbursts consist of mild state with a limiting intrinsic surface brightness $L_{bol}r_e^{-2} \simeq 10^{12} L_{\odot} \text{ kpc}^{-2}$ and intense state with a characteristic scale of $r_e \simeq 0.3 \text{ kpc}$. The mild starburst can be triggered by the disc instability as proposed by Meurer et al. (1997). For ULIRGs, the surface brightness is an order of magnitude larger than that of UVSBGs. A simple analysis of the feedback allows us to derive a critical luminosity over which starburst regions cannot be sustained by the feedback against self-gravity. This limitation of the feedback causes the bimodality of starburst activity, in which the size of starburst region has a clear limit of $r_e \simeq 0.3 \text{ kpc}$. According to this analysis, all of the ULIRG sample is identified as self-gravity dominated starbursts. Furthermore, we compare the velocity dispersions inferred from the SED fitting results with observations to find that starburst regions in ULIRGs are dynamically unstable. In order to produce the dynamically unstable starbursts with strong mass concentration, a violent trigger mechanism is required, rather than the disc instability. As suggested by various imaging observations, the most plausible trigger mechanism of ULIRGs would be galaxy merging which can cause the dynamical disturbance over a galactic scale.

ACKNOWLEDGEMENTS

TT would like to thank to N. Shibazaki, V. Vasevičius, T. Matsumoto and M. Rowan-Robinson for their encouraging supports. We would like to thank the anonymous referee for the sensible comments. We are grateful to C. Pearson for his careful reading of the draft. This work was financially supported in part by a Grant-in-Aid for the Scientific Research (No.11640230, 13011201 & 14540220) by the Japanese Ministry of Education, Culture, Sports and Science. This research has been supported in part by a Grant-in-Aid for the Center-of-Excellence (COE) research. Also, TT acknowledges the support of PPARC. We acknowledge the use of Lyon-Meudon Extragalactic Database (LEDA). This research has made use of the NASA/IPAC Extragalactic Database (NED) which is operated by the Jet Propulsion Laboratory, California Institute of Technology, under contract with the National Aeronautics and Space Administration.

REFERENCES

- Adelberger K.L., Steidel C.C. 2000, ApJ, 544, 218
 Alonso-Herrero A., Engelbracht C.W., Rieke M.J., Rieke G.H., Quillen A.C. 2001, ApJ, 547, 129
 Arimoto N., Yoshii Y. 1987, A&A, 173, 23
 Arimoto N., Yoshii Y., Takahara F. 1992, A&A, 253, 21
 Armus L., Heckman T.M., Miley G.K. 1990, ApJ, 364, 471
 Bryant P.M., Scoville N.Z. 1999, AJ, 117, 2632
 Calzetti D., Bohlin R.C., Kinney A.L., Storchi-Bergmann T., Heckman T.M. 1995, ApJ, 443, 136
 Calzetti D., Kinney A.L., Storchi-Bergmann T. 1994, ApJ, 429, 582
 Combes F., Boissé P., Mazure A., Blanchard A. 1995, in *Galaxies and Cosmology* (Springer-Verlag, Berlin Heidelberg) p. 96
 Dikey J.M., Hanson M.M., Helou G. 1990, AJ, 99, 1071
 Dwek E. 1998, ApJ, 501, 643
 Fioc M., Rocca-Volmerange B. 1997, A&A, 326, 950
 Genzel R., Lutz D., Sturm E., Egami E., Kunze D., Moorwood A.F.M., Rigopoulou D., Spoon H.W.W. et al. 1998, A&A, 498, 579
 Goldader J.D., Meurer G., Heckman T.M., Seibert M., Sanders D.B., Calzetti D., Steidel C.C. 2002, ApJ, 568, 651
 Gordon K.D., Calzetti D., Witt A.N. 1997, ApJ, 487, 625
 Heckman T.M., Lehnert M.D., Stickland D.K., Armus L. 2000, ApJS, 129, 493
 Heckman T.M., Robert C., Leitherer C., Garnett D.R., van der Rydt F. 1998, ApJ, 505, 174
 James P., Bate C., Wells M., Wright G., Doyon R. 1999, MNRAS, 309, 585
 Kennicutt R.C. 1989, ApJ, 344, 685
 Kennicutt R.C. 1998, ApJ, 498, 541
 Kinney A.L., Bohlin R.C., Calzetti D., Panagia N., Wyse R.F.G. 1993, ApJS, 86, 5
 Kobulnicky H.A., Gebhardt K. 2000, AJ, 119, 1608
 Kodama T., Arimoto N. 1997, A&A, 320, 41
 Lehnert M.D., Heckman T.M. 1996, ApJ, 472, 546
 Leitherer C., Heckman T.M. 1995, ApJS, 96, 9
 Lequeux J., Peimbert M., Rayo J.F., Serrano A., Torres-Peimbert S. 1979, A&A, 80, 155
 Lutz D., Spoon H.W.W., Rigopoulou D., Moorwood A.F.M., Genzel R. 1998, ApJ, 505, L103
 McQuade K., Calzetti D., Kinney A. 1995, ApJS, 97, 331
 Meurer G.R., Heckman T.M., Leitherer C., Kinney A., Robert C., Garnett D.R. 1995, AJ, 110, 2665

- Meurer G.R., Heckman T.M., Lehnert M.D., Leitherer C., Lowenthal J. 1997, *AJ*, 114, 54
- Meurer G.R., Heckman T.M., Calzetti D. 1999, *ApJ*, 521, 64
- Pagal B.E.J. 1997, in *Nucleosynthesis and Chemical Evolution of Galaxies* (Cambridge University Press, Cambridge) p. 82
- Pei Y.C. 1992, *ApJ*, 395, 130
- Prugniel Ph., Heraudeau Ph. 1998, *A&AS*, 128, 299
- Quirk W.J. 1972, *ApJ*, 176, L9
- Rigopoulou D., Lawrence A., Rowan-Robinson M. 1996, *MNRAS*, 278, 1049
- Rigopoulou D., Spoon H.W.W., Genzel R., Lutz D., Moorwood A.F.M., Tran Q.D. 1999, *AJ*, 118, 2625
- Rowan-Robinson M., Efstathiou A. 1993, *MNRAS*, 263, 675
- Sanders D.B., Scoville N.Z., Soifer B.T. 1991, *ApJ*, 370, 158
- Sanders D.B., Soifer B.T., Elias J.H., Madore B.F., Matthews K., Neugebauer G., Scoville N.Z. 1988, *ApJ*, 325, 74
- Scoville N.Z., Evans A.S., Thompson R., Reike M., Hines D.C., Low F.J., Dinshaw N., Surace J.A. et al. 2000, *AJ*, 119, 991
- Shier L.M., Fischer J. 1998, *ApJ*, 497, 163
- Soifer B.T., Neugebauer G., Matthews K., Egami E., Becklin E.E., Weinberger A.J., Ressler M., Werner M.W. et al. 2000, *AJ*, 119, 509
- Storchi-Bergmann T., Calzetti D., Kinney A.L. 1994, *ApJ*, 429, 572
- Sullivan M., Treyer M.A., Ellis R.S., Bridges T.J., Millard B., Donas J. 2000, *MNRAS*, 312, 442
- Surace J.A., Sanders D.B. 2000, *AJ*, 120, 604
- Takagi T. 2001, PhD thesis, Rikkyo Univ.
- Takagi T., Arimoto N., Vansevicius V. 1999, *ApJ*, 523, 107
- Toomre A. 1964, *ApJ*, 139, 1217
- Trentham N., Kormendy J., Sanders D.B. 1999, *AJ*, 117, 2152
- Veilleux S., Kim D.-C., Sanders D.B. 1999a, *ApJ*, 522, 113
- Veilleux S., Sanders D.B., Kim D.-C. 1999b, *ApJ*, 522, 139
- Witt A.N., Gordon K.D. 2000, *ApJ*, 528, 799
- Wynn-Williams C.G., Becklin E.E. 1993, *ApJ*, 412, 535